THERMAL MANAGEMENT OF PHOTOVOLTAIC PANELS UTILIZING SOLID-SOLID PHASE CHANGE MATERIAL

A THESIS SUBMITTED TO
THE GRADUATE SCHOOL OF NATURAL AND APPLIED SCIENCES
OF
MIDDLE EAST TECHNICAL UNIVERSITY

BY

ÇETİN AKÇAY

IN PARTIAL FULFILLMENT OF THE REQUIREMENTS
FOR
THE DEGREE OF MASTER OF SCIENCE
IN
MECHANICAL ENGINEERING

DECEMBER 2024

Approval of the thesis:

THERMAL MANAGEMENT OF PHOTOVOLTAIC PANELS UTILIZING SOLID-SOLID PHASE CHANGE MATERIAL

submitted by **ÇETİN AKÇAY** in partial fulfillment of the requirements for the degree of **Master of Science** in **Mechanical Engineering, Middle East Technical University** by,

Prof. Dr. Naci Emre Altun
Dean, **Graduate School of Natural and Applied Sciences** _________________

Prof. Dr. Serkan Dağ
Head of the Department, **Mechanical Engineering** _________________

Assoc. Prof. Dr. Özgür Bayer
Supervisor, **Mechanical Engineering, METU** _________________

Examining Committee Members:

Prof. Dr. Zafer Dursunkaya
Mechanical Engineering, METU _________________

Assoc. Prof. Dr. Özgür Bayer
Mechanical Engineering, METU _________________

Prof. Dr. Abdullah Ulaş
Mechanical Engineering, METU _________________

Assoc. Prof. Dr. Onur Taylan
Mechanical Engineering, METU _________________

Prof. Dr. Murat Köksal
Mechanical Engineering, Hacettepe University _________________

Date: 27.12.2024

I hereby declare that all information in this document has been obtained and presented in accordance with academic rules and ethical conduct. I also declare that, as required by these rules and conduct, I have fully cited and referenced all material and results that are not original to this work.

Name Last name : Çetin Akçay

Signature :

ABSTRACT

THERMAL MANAGEMENT OF PHOTOVOLTAIC PANELS UTILIZING SOLID-SOLID PHASE CHANGE MATERIAL

Akçay, Çetin
Master of Science, Mechanical Engineering
Supervisor : Assoc. Prof. Dr. Özgür BAYER

December 2024, 85 pages

Renewable energy generation has gained increasing attention in recent years. One of the renewable energy resources is solar power. Photovoltaic panels are employed to produce electricity with solar irradiance. However, the electrical conversion of photovoltaic panels is not efficient. Cooling photovoltaic panels may be a solution to increase the efficiency of them. For thermal management, one of the remarkable methods is the use of phase change materials. Mostly used phase change materials are solid-liquid phase change materials although they have low thermal stability and proper shape. On the other hand, solid-solid phase change materials are an effective alternative in terms of their heat absorption capacity, proper shape, and thermal stability. Those materials keep their solid phase after phase transition at a specific temperature interval. The material absorbs energy during its phase change. In this thesis, the implementation of solid-solid phase change material to the photovoltaic panel is investigated experimentally and numerically. Experimental outputs are used as input in the simulations and their results are used to validate numerical models. Different solid-solid phase change material configurations are investigated numerically to increase the efficiency of photovoltaic panels. Numerical results showed that the use of solid-solid phase change material with photovoltaic panel has improved its performance. Average temperature of photovoltaic panel top surface decreased 9.74%. As an ideal design, the phase change material which has 40 mm thickness contributed to the average efficiency of the photovoltaic panel by increasing it from 9.05% to 9.27%.

Keywords: Photovoltaic Panels, Solid-Solid Phase Change Materials, Neopentyl Glycol, Experiment, Numerical Simulations

ÖZ

KATI-KATI FAZ DEĞİŞİM MALZEMESİ KULLANAN FOTOVOLTAİK PANELLERİN ISIL YÖNETİMİ

Akçay, Çetin
Yüksek Lisans, Makina Mühendisliği
Tez Yöneticisi: Doç. Dr. Özgür Bayer

Aralık 2024, 85 sayfa

Yenilenebilir enerji üretim yöntemleri son yıllarda daha da dikkat çekmeye başlamıştır. Bu yenilenebilir enerji yöntemlerinden biri de güneş enerjisinin kullanımıdır. Güneş enerjisini elektrik enerjisine dönüştürmek için fotovoltaik paneller kullanılmaktadır. Ancak, bu paneller yeterince verimli çalışmamaktadırlar. Hatta, çalışma sıcaklıkları arttıkça verimleri daha da düşmektedir. Bu yüzden, panellere uygulanabilecek bir ısıl yönetim panellerin verimliliğini arttırabilir. Dikkat çeken ısıl yönetim yollarından biri faz değiştiren malzemelerin kullanımıdır. Çoğunlukla katı-sıvı faz değiştiren malzemeler kullanılmasına rağmen; bu malzemeler düşük termal kararlılığa ve eridikleri için belirsiz bir şekle sahiptirler. Katı-katı faz değiştiren malzemelerse, belli bir sıcaklık aralığında kristal yapılarını değiştirerek enerji depolarlar ve ısıl yönetim sağlamış olurlar. Bunu yaparken şeklini ve termal kararlılığını korumaya devam ederler. Bu tezde, katı-katı faz değiştiren malzeme ile fotovoltaik panelin birlikte kullanımı incelenmiştir. Araştırma için deney yapılmış olup deney sonuçları kurulan sayısal modelin geçerliliğinin tespitinde kullanılmıştır. Kurulan sayısal model bu sayede farklı katı-katı faz değiştiren malzeme konfigürasyonlarında da kullanılmış olup panellerin ısıl yönetimi ve enerji üretimi incelenmiştir. Testlerden toplanan verilerin kullanılmasıyla gerçekleştirilen sayısal analizler sonucunda katı-katı faz değiştiren malzemenin kullanımın fotovoltaik panel performansını geliştireceği gösterilmiştir. Fotovoltaik panelin üst yüzey sıcaklık ortalaması %9.74 düşmüştür. İdeal bir çözüm olarak da 40 mm kalınlığa sahip faz değiştiren malzeme fotovoltaik panelin verimliliğini %9.05'ten %9.27'ye arttırmıştır.

Anahtar Kelimeler: Fotovoltaik Panel, Katı-Katı Faz Değiştiren Malzemeler, Neopentil Glikol, Deney, Sayısal Simülasyonlar

To my family…

ACKNOWLEDGMENTS

I would like to express my deepest gratitude to his supervisor Assoc. Prof. Dr. Özgür BAYER for their guidance, advice, criticism, encouragements and insight throughout the research.

I would like to thank my friends Berkay FİLİZ and Dünya Berrak KUTLUTÜRK for their support all the time.

Finally, I would like to express my deepest love to my parents Hale AKÇAY and Gökhan AKÇAY for their unconditional love, support and encouragement along the way.

TABLE OF CONTENTS

LIST OF TABLES

TABLES

LIST OF FIGURES

FIGURES

LIST OF ABBREVIATIONS

ABBREVIATIONS

3-D	3 Dimensional
CFD	Computational Fluid Dynamics
EVA	Ethylene Vinyl Acetate
NPG	Neopentyl Glycol
PCM	Phase Change Material
PV	Photovoltaic
SL-PCM	Solid-Liquid Phase Change Material
SS-PCM	Solid-Solid Phase Change Material

LIST OF SYMBOLS

SYMBOLS

α	Absorptivity, Thermal diffusivity (m^2/s)
h	Convective heat transfer coefficient (W/m^2K)
ρ	Density (kg/m^3)
η	Efficiency
ε	Emissivity
g	Gravitational acceleration (m/s^2)
I	Irradiance (W/m^2)
ν	Kinematic viscosity (m^2/s)
L	Latent heat (kJ/kg)
Nu	Nusselt Number
β	Phase change fraction, Thermal expansion coefficient $(1/K)$
P	Power (W)
Pr	Prandtl number
Ra	Rayleigh Number
R	Resistance (Ω)
C_p	Specific heat capacity, (kJ/kgK)
σ	Stefan-Boltzmann coefficient (W/m^2K^4)
T	Temperature, (^{o}C or K)
k	Thermal conductivity, (W/mK)

d	Thickness, (mm)
τ	Transmissivity
$\dot{q}$	Volumetric heat source (W/m^3)

CHAPTER 1

INTRODUCTION

World's energy consumption is increasing day by day and this situation brings the need of higher energy generation along with it. In order to fulfill the energy demand of the growing population, fossil fuel usage is the first choice of the people although it has extreme negative effects on the environment [1]. Climate change and pollution of nature are the main disasters which are caused by the consumption of fossil fuels. Efforts to decrease the use of them canalizes people to acquire the needed energy from renewable energy resources. Renewable energy resources can be listed as wind, solar energy, hydroelectric, geothermal, biomass and tidal energy.

Solar energy is an important alternative to the conventional electricity production methods as it is a simple technology and environmentally friendly [2]. Since it is a cleaner way to obtain the demanded energy, people focus on the use of it alternatively, in their houses or in the industries. However, solar energy is still not a cost-effective solution as an alternative power generation method [3]. In order to exceed the lack of energy problem of the world, one of the things that the researchers focused on is how to improve efficiency of the obtained energy from the solar panels.

Efficiency of the solar panels are the main problem which is dealt with by the researchers. Photovoltaic cells absorb 80% of the coming solar irradiation and transforms the small part, which is 15% or 20%, of it to electricity, the most of the incident energy is turned to the heat [4]. Panel temperatures get much higher than the environment and this increase of temperature of the solar panel creates an inefficient condition in terms of converting solar irradiation into electricity. Known efficiency values of the industrial photovoltaic cells belong to the measurements which were done under standard conditions [4]. In other words, given data does not belong to exact working conditions of the photovoltaic cells. Every 1℃ temperature increase on the surface of photovoltaic cell causes the decline of electrical efficiency of panel up to 0.045% [5].

Use of photovoltaic cells is a great alternative to supply the demanded electrical energy of the world. Therefore, studies are focused on increasing the efficiency of the photovoltaic cells. To enhance the performance of photovoltaic cells, researchers explore various methods to reduce temperature rise under solar irradiation, as increased temperatures lead to decreased efficiency. Therefore, in order to decrease the increased temperatures on the cells, various cooling methods are proposed to be applied to the photovoltaic panels.

Active cooling and the passive cooling are the two main strategies for thermal management. Active cooling methods include fluid flow such as air or water etc. in order to dissipate heat [6]. Circulating the fluid flow through the photovoltaic cell could be realized by an external pump or fan. To clarify, cooling of the photovoltaic cells is realized by forced convection and since forced convection requires pumps or fans, they cause additional consumption of the energy.

Another approach to the cooling implementations is the passive cooling. Passive cooling relies on natural convection and conduction to dissipate heat from the source [5]. These methodologies do not consume energy to enable the extraction of heat. Natural convection on a surface may not be enough in order to improve the performance of the passive cooling methods, fins and phase change materials can be implemented, which are some of the most popular methods, nowadays. Mounting fins to the photovoltaic cells causes that fins absorb the accumulating heat and remove it by conduction. Phase change materials have high capacity latent energy during their melting process with small temperature increase [7]. Phase change materials (PCM) absorb the heat coming from heat source. During the absorption, the temperature of PCM starts to increase and PCM stores the energy as latent heat at a certain temperature interval. Phase transition of PCMs is depicted in Figure 1.1. PCMs have great potential to absorb large quantities of energy. Solid-liquid phase change materials (SL-PCM) are the most used ones among PCMs. PCM starts melting at a certain temperature interval during charging period. Although the temperature change of the material is extremely small, it absorbs much energy during melting. Therefore, the idea of using PCMs in areas requiring thermal management has come to the forefront and photovoltaic panels are one of those areas. Phase change materials, by absorbing heat, offer exceptional thermal energy storage capacity while effectively managing the temperature of photovoltaic panels. Moreover, there is another type of phase change materials which is not melting during phase change. Those materials are called solid-solid phase change materials (SS-PCM). SS-PCMs have certain phase transition temperature like the other phase change materials. However, they remain solid during this process. SS-PCMs have high latent capacity with a small temperature rise during phase change which is transition from alpha phase to gamma phase of materials [8]. SL-PCMs have leakage risk or they have changing thermal properties with respect to temperature. However, SS-PCMs do not have those problems due to remaining at solid phase and protecting its thermal stability. SS-PCM may be a useful alternative to SL-PCMs because they have high thermal stability, limited volume expansion during heating, low subcooling and significant latent heat.

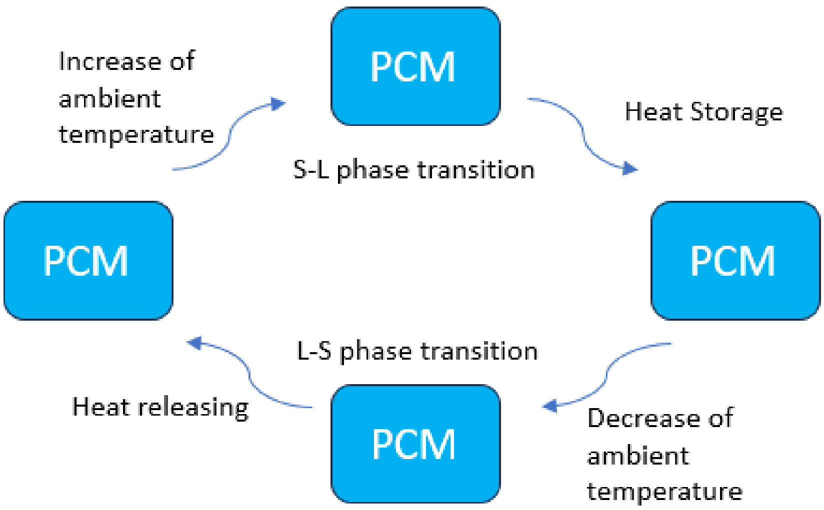

Figure 1.1 Scheme of Phase Transition of Solid-Liquid Phase Change Materials, adapted from [9]

SS-PCM integration to the photovoltaic (PV) panel is investigated by Pillai et al. [10] recently in the literature will be examined in this study. Active cooling methods have drawbacks such as high energy consumption, maintenance needs, and limited cost-effectiveness. To overcome these and address issues with solid-liquid phase change materials, such as leakage and difficult encapsulation, solid-solid phase change materials will be implemented on photovoltaic panels.

1.1 Literature Review

Several methodologies are employed to provide thermal management to PV panels since as much as operating temperature of PV panel increases, energy conversion efficiency decreases. Aim of the applications is to improve the dissipated heat transfer rate from the PV panel. Therefore, different active and passive cooling methodologies are investigated in the literature.

1.1.1 Photovoltaic Panel Thermal Management without PCM

Thermal management could improve the electrical conversion efficiency of the PV panels. Some methodologies are followed in order to improve their electrical conversion efficiency. Hussien et al. [3] investigated increasing power output, panel efficiency and life time of the PV panel by applying forced convection on the photovoltaic panel experimentally and numerically. Three different cases which are a case without cooling, duct integrated photovoltaic panel by providing forced convection with a blower on the back surface of the panel and small fans integrated panel on the back surface were observed experimentally. Experiments were done on a sunny day in Autumn. The results of the experiments showed that, small fans integrated photovoltaic panel system has shown a raise of generated power 12.3%. Blower integrated photovoltaic panel increased the generated power of the photovoltaic panel 7.1%. Moreover, researchers created a numerical model by using a commercial CFD software. Their results showed that outputs of the numerical analysis are validated by experimental results. Validation gives that numerical model may be implemented for different PV panel application without realizing experiments.

The impact of air velocity passing through the photovoltaic panel was investigated by Ali et al. [11] experimentally and numerically. Air with a velocity ranging from 0 to 15 m/s was directed through the PV panel in a laboratory setting. It was found that increasing value of air velocity causes raise in the electrical efficiency of the panel. Moreover, the tilt angle of the panel is changed from 0^o to 10^o. When the air flows through the panel on tilted angle, the air flow increases the electrical efficiency of the panel more than the parallel flow to the surface of the PV panel.

Different cooling channel geometries with air on the back surface of the photovoltaic panel is investigated by Özcan et al. [12]. Annual irradiation and temperature data are collected and electricity generation is calculated. Collected data is used in order to analyze different cooling channels on a commercial CFD software. In the simulations, flat channels and curved finned channels are modelled. Cell temperatures, cooling rates and pressure drop are calculated for different air velocities in the cooling channel. The best cooling performance is acquired by the curved fin configuration. However, when the fan power electricity consumption is taken into account, the best configuration is the one with the flat fins.

The use of water-jet impingement to address the temperature rise in photovoltaic panels is studied by Javidan et al. [13]. The study is realized by changing four different parameters which are number of nozzles, nozzle diameter, flow rate and nozzle-to-panel spacing. Investigation is concluded experimentally and result of the experiments are used to achieve optimum design configuration by using response surface methodology. Increase in flow rate and number of nozzles improve the performance of the PV panel and increase in diameter and nozzle-to-panel spacing decreases performance. Optimum design maximizes efficiency and its output power is boosted 47.67%. The best temperature uniformity is obtained by minimum nozzle-to-panel spacing, minimum diameter and maximum number of nozzles. In a numerical investigation, Mohammadpour et al. [14] investigated same parameters in the research of Javidan et al. [13] by using nano-fluid for the jet-cooling methodology. In this study, the case is studied numerically. Results proved that nano-fluid jet impingement configuration improved the thermal management of PV panel and performance of it.

Cooling of PV panels with fins is worked on by Shiravi et al. [15]. Experiments are realized by mounting aluminum fins on the back surface of the photovoltaic panel. Temperature drop is observed with use of aluminum fins, since aluminum fins create more convection on the back surface of the PV panel. Moreover, entropy analysis is done for conventional PV panel and finned PV panel. That entropy generation of finned configuration is less than the conventional one is reached. Therefore, it may be said that improving the performance of PV panel is important in terms of the environment.

Effect of the attachment of the fins to the thermal management of the PV panels is examined by Elsafi et al. [16]. Numerical analysis is realized in order to figure out the performance of different fin configurations which are straight fins and pin fins. Although the performance differences among straight fin types were minimal, rectangular fins proved to enhance the electrical efficiency of the PV panel the most. Further, different fin materials with different fin types may present an optimum solution and improving electrical efficiency of the PV panels. The study showed that pin fins are the most beneficial configuration in terms of enhancing the electrical efficiency of a PV panel.

Influence of fin height to the heat dissipation from PV panels is inspected by Del Rio et al. [17]. The integration of fins to the PV panels is worked numerically in order to provide temperature control to them. To realize their study, a commercial CFD program is used. Different fin heights were the research topic. As a result of their investigation, if the fin height increases, operating temperature of photovoltaic panel decreases. Thus, electrical generation of photovoltaic panel may improve.

In a numerical study, effects of solar irradiance, ambient temperature and wind velocity for a water cooled PV panel is investigated by Wu et al. [18]. Different solar irradiance, ambient temperature and wind velocity values are used during the simulations. Water cooling on PV panel shows more effective performance during high solar irradiation. When the ambient temperature and solar irradiation are at the largest, water cooling provides great enhancement of the efficiency of the PV panel.

A spiral cooling pipe integrated to PV panel is investigated by Rosli et al. [19] numerically. The aim of the study is that improving the temperature uniformity on PV panel while decreasing operating temperature of it, since non-uniformity causes lower efficiency on some location of panel. Non-uniformity may cause thermal stresses on photovoltaic panel and the panel may be damaged. Therefore, a spiral pipe is designed to be mounted on the back surface of PV panel. The numerical model is validated by another experimental results and results of spiral pipe model are compared with those experimental results. Custom spiral pipe design has contributed to thermal management. Temperature uniformity of the photovoltaic panel is better than the conventional straight pipe. Therefore, that design may provide higher electrical output.

Cooling of photovoltaic cells by applying nano-particle included water through tubes on the back surface is studied by Babavali et al. [20] experimentally. Ingredient of the water is MgO. Results of the experiments showed that conventional photovoltaic panel's temperature reached 78℃. However, cooled PV panel with nano-particled water reached 35℃. Since, electrical efficiency of PV panels declines with raising panel temperature, the experiments presented that nano-MgO/water cooling on photovoltaic panels is beneficial. The electrical efficiency of the PV panel has shown 16.9% enhancement.

Operating temperature of photovoltaic panels is analyzed numerically using a water-based nanofluid containing single-walled carbon nanotubes by Sharifpur et al. [21]. Different volume fractions of single walled carbon nano-tubes are tested in order to provide thermal management to the PV panels. However, there was not remarkable advantage of use of single walled carbon nano-tube. When sensitivity analysis is realized between solar radiation, volume fraction of single walled carbon nano-tube, ambient temperature and mass flow rate, it was found that the largest impact on a solar panel is sourced by solar radiation.

Introduced cooling methodologies without PCM are efficient. However, some of them are traditional methodologies which can be improved or some of them consume energy while cooling the panels. Advancing those ways for thermal management of PV panels encourages researchers and do further researches on those.

1.1.2 Photovoltaic Panel Thermal Management with PCM

New approaches are explored to improve the traditional cooling methodologies Therefore, a novel method that enhances passive techniques while avoiding power consumption associated with active methods has garnered attention. Therefore, phase change materials involved in heat dissipation process of photovoltaic panels.

Savvakis et al. [22] investigated the effects of a phase change material on electrical output performance of a PV panel, since operation temperature of PV panel is a critical parameter which influence the performance of it. The study is done experimentally by observing conventional PV panels and PV panel with phase change material which is RT27. SL-PCM was placed into a container and then container was mounted to the back surface of PV panel. Current – voltage and glass top surface temperature data are collected for both configurations. It was found that SL-PCM has positive effect in terms of decreasing operating temperature of PV panel. This means that improvement in electrical energy generation of PV panel. Additionally, a life cycle assessment analysis is realized for the SL-PCM and PV panel configuration. It is reached that metal container has the greatest impact on the environment for this configuration with respect to other components of the system.

The cooling of photovoltaic panel by using two different SL-PCMs which are RT28 and RT35 is studied by Aneli et al. [23] numerically. Two dimensional simulations are run in order to see the effect of utilization of different SL-PCMs. In the simulations, both materials have contributed to decreasing the operating temperature of the photovoltaic cells. However, during the 24-hour simulations, RT28 did not convert back to solid phase in its cooling time interval. Therefore, while simulating RT28, the numerical analysis procedure should be extended to 48-hour for similar environmental conditions. The use of both SL-PCMs was found to positively impact the reduction of the PV panel's operating temperature, resulting in higher electrical output at different times throughout the year.

Integrating two different SL-PCMs to a PV panel is studied by Ma et al. [24] in order to show decrease of operating temperatures. As a result of the two-dimensional numerical analysis, both SL-PCMs develop the decline of the temperature of the PV panel. Moreover, it is detected that the SL-PCM which has lower melting point temperature kept the temperature of the PV panel for a longer time under a certain temperature than the other SL-PCMs. Therefore, it may be said that, the PCM which has lower melting point may provide higher electrical energy in the environmental conditions of those simulations.

In a numerical study, Bria et al. [25] investigated the effect of SL-PCM thickness in a finned photovoltaic panel configuration. Six different SL-PCM thicknesses are simulated. RT42 is used as SL-PCM. In order realize the analysis more realistic, weather condition data of a location in Morocco is used. Results of the simulations indicates that increasing SL-PCM thickness drops the operating temperature of PV panels. In the study, the largest two SL-PCM thicknesses do not give much different results. Therefore, the largest second thickness is selected for use.

The effect of thermophysical properties of SL-PCMs to the thermal management and efficiency of PV panel is investigated by Abd El-Hamid et al. numerically [26]. This study verified that integration of SL-PCM decreases surface temperature of PV panel and overall energy efficiency increases.

PCM types and their container shapes are research areas in passive cooling methodologies. Navarro et al. [4] studied the effect of SL-PCM type and shape of the PCM container to the operating temperatures and electrical efficiency of photovoltaic panel. Two-dimensional simulations are done for the investigation on a commercial CFD software. Their study showed the positive impact of integrating SL-PCM to the efficiency of the panel. Trapezoidal box for SL-PCM presents better performance than the rectangular shaped box. Moreover, if the melting temperature of the SL-PCM is lower than the average ambient temperature, the performance of the PV panel even gets better.

Investigation of Kumar et al. [5] is on the comparison between conventional PV panel and PV panel with copper and SiC included SL-PCM. This mixture of SL-PCM is integrated to the PV panel. The study is conducted experimentally. Aim of the adding particles to the SL-PCM is increasing the thermal conductivity of it. Results showed that integration of combined SL-PCM contributed to the dropping operating temperature of the PV panel and improving the electrical efficiency 4.3%.

The electrical conversion performance of the PV panels with using SL-PCM and aluminum plate is researched by Rajvikram et al. [27] at the backside of the panel. As already mentioned, PCM is used for absorbing the heat and aluminum plate is used for dissipating the heat to the environment with higher rate. Results proved that average temperature on the PV panel decreased 10.35℃ and electrical efficiency of the panel increased 2%.

In an experimental study, Marudaipillai et al. [28] investigated the effect of SL-PCM and graphite mixture to the heat removal from a PV panel. A material is synthesized for the investigation by the researchers. Synthesized material is embedded into the fin structure on the back of the PV panel. Expanded graphite improves the thermal conductivity and physical form of the SL-PCM. Implemented method to improve thermal management of PV panel raised the electrical efficiency of the panel 3.67% with respect to conventional PV panels.

The thermal regulation of PV panels with SL-PCM infused graphite and aluminum heat sink is inspected by Atkin et al. [29] experimentally and numerically. Different configurations are tested, which are conventional PV panel, PV panel with SL-PCM infused graphite, PV panel with aluminum fins and PV panel with aluminum fins and SL-PCM infused graphite. Numerical analysis is validated with experimental results. Numerical analysis is done with 1-D modelling through numerical competing program. The results showed that the case with aluminum fins and PCM infused graphite improved the electrical efficiency of the PV panel from 13.2% to 14.92% with respect to reference case which does not have thermal regulation.

Improving a mathematical modelling methodology is investigated by Tao Ma et al. [30]. This methodology is to make easier to realize the thermal design of the PV panel with SL-PCM. A sensitivity analysis is realized on the parameters which effects the performance of photovoltaic cells by using developed one-dimensional thermal circuit model. Results of the study indicated that every 100 W/m^2 increase in irradiation causes 5℃ increase in the peak temperature of the PV panel. Moreover, it was found that optimum PCM melting temperature is 5℃ higher than the average ambient temperature.

A mathematical model is developed to predict the behavior of PV panel with SL-PCM by Durez et al. [31] in order to provide thermal management to the panel. Validation of the mathematical model is followed by the prediction of the correct PCM to a specific climate zone. In order to do that a genetic algorithm application is done on a numerical computation program. In the simulations, it is reached that a PCM which has melting point as 21℃ contrubitued to that the maximum panel temperature dropped from 65℃ to 38℃ and that efficiency of the panel increased 6%.

Al Najjar et al. [32] conducted a study aimed at formulating an innovative mathematical framework for cooling investigation of PV panels, in order to eliminate the computational fluid dynamics calculation time and cost. The PV panel configuration includes PCM. Founded model is validated by computational fluid dynamics and an experiment. Extreme decline of computational time cost is reached.

Experiments are performed by Abdelrahman et al. [33] to investigate the effect of adding Al_2O_3 nanoparticles into the SL-PCM of PV panel. An aluminum plate is used in order to simulate the PV panels during the experiments. Fins are used as thermal conductivity enhancers in the configuration. Increasing the volume fraction of nanoparticles up to 0.77% decreases the surface temperature of the plate.

The influence of SL-PCM embedded aluminum foam to the cooling performance of PV panels is observed by Sharaf et al. [34]. The experiments are done in winter. Temperature data and electricity generation data has been collected during the experiments. It was found that the metal foam-PCM configuration has significant effect on the heat dissipation from the PV panels. The configuration made the PV panel raise the electricity generation up to 4.14%. This value means that power generation is higher than the conventional PV panel's generation.

Use of SS-PCM with PV panels is suggested by Pillai et al. [10] to increase the power generation performance of PV panels. In their recent study, An experimental study is conducted to examine the impact of solid-solid phase change material on the performance of PV panels. In order to increase the thermal conductivity of the PCM, they added Al_2O_3 inside of it. Characterization of the synthesized material are obtained from thermogravimetric analysis, fourier-transform infrared spectroscopy, differential scanning calorimetry and t-history analysis. In the study, the cases which are conventional PV panel, PV panel with pure NPG and PV panel with NPG+Al_2O_3 are compared. Results showed that addition of NPG increased generated power and addition Al_2O_3 to the NPG caused better performance improvement.

1.2 Motivation

Many studies about the thermal management methodologies of the PV panels are introduced in the literature survey section. Some of them used active cooling methods which employ the fluid by implementing forced convection on the system. Although the concept of forced convection aids in the thermal regulation of the system, it requires an external power supply and consumes energy. Passive methods are applied such as fins and solid-liquid phase change materials together in some of the investigations. This is a useful way to improve the efficiency of the photovoltaic panel. However, it has some deficiencies in terms of use. SL-PCMs have some encapsulation problems, or leakage problems. Moreover, since thermal properties of solid-liquid phase change materials change with temperature, this condition create challenges for the designers.

The SS-PCMs are employed to show that they can contribute to cooling of the PV panels in this thesis. Although Pillai et al. [10] have done similar research recently, their research is just an experimental evaluation. The stated problem in the thesis is examined both experimentally and numerically. Moreover, thermal characterization is done for PCM and suitable PCM thickness for a PV panel is determined.

SS-PCMs keep their current phase which means stays solid, the design does not have special encapsulation and leakage problem like solid-liquid phase change material. Moreover, those materials do not have thermal properties changing with temperature. As a result, SS-PCMs promise thermally more stable designs to the users.

As a result, the low efficiency of photovoltaic panels is a topic that requires further research and offers opportunity for improvement. As mentioned in the literature review, many different methods have been tried, yielding various contributions. As explained, SS-PCM is a passive cooling approach that could contribute to the development of photovoltaic panels. Therefore, this thesis will examine the contribution of this alternative method to the thermal management of photovoltaic panels.

1.3 Problem Statement and Objective

The focus of the thesis is to examine the impact of using SS-PCM with PV panels to achieve temperature control and enhance their electrical conversion efficiency.

SS-PCMs are chosen to be applied to the PV panels, due to their ability of storing the thermal energy as latent heat within a specific temperature range while remaining solid after the phase change. Having a material with high latent heat on the PV panels can provide effective heat removal them. Additionally, since the material retains its solid state, it eliminates the need for special encapsulation and avoids leakage issues typically associated with SL-PCMs.

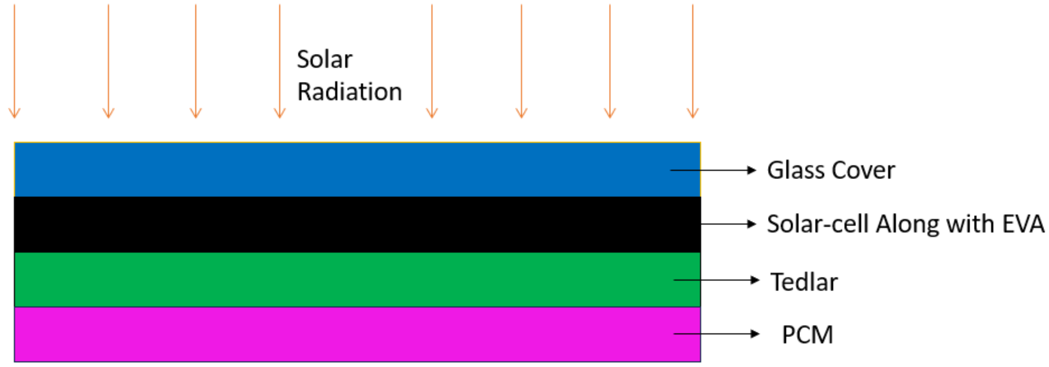

Figure 1.2 PV Panel with Phase Change Material (PCM), adapted from [31]

Schematic view of a PV panel with PCM is depicted in Figure 1.2. Solar radiation is transmitted through the glass layer to the solar cell area which is silicon. Ethylene vinyl acetate (EVA) is used as adhesive for solar cell to the glass and tedlar. Tedlar is a protection cover at the backside of the cells. In this figure, there is a PCM layer at the backside of the cell. In this thesis, there will be SS-PCM which is neopentyl glycol (NPG). Chemical formula of NPG is $C_5H_{12}O_2$. Material properties of NPG is indicated in Table 1.1.

Table 1.1 Material Properties of Neopentyl Glycol

Property	**Value**
$\rho\ (kg/m^3)$	1060 [35]
$c_p\ (kJ/kgK)$	2.516 [35]
$k\ (W/mK)$	0.24 [36] 0.15-0.42 [37]
Transition Temperature (℃)	41-46.4 [38,39]
L (kJ/kg)	131.9 [36]

Neopentyl glycol is a material which has a phase transition between the interval of 41℃ to 46.4℃, however it keeps its solid form. Although it has a melting point, the material has much higher energy absorption capacity than the melting during solid-solid phase change. There are different thermal conductivity values changing between 0.15 W/mK to 0.42 W/mK [37].

This material includes many hydrogen bonds in it. NPG has larger enthalpy change during solid-solid phase change than its solid-liquid phase change. Low-temperature monoclinic α form changes to high temperature phase, γ phase, during solid-solid phase change This phase transition is kept company by partly breaking of the hydrogen bonds [38]. The differential scanning calorimeter is used to examine the thermal characteristics and phase change properties of the materials. This device is used to detect the phase transition temperature and latent heat of the NPG in Wang et al. [38]'s study. The thermal behavior of the SL-PCM while it is being heated is represented in Figure 1.3. Since there is not a specific nomenclature for phase transition temperatures of SS-PCM, Figure 1.3 is presented. SS-PCM shows similar thermal behavior in certain temperature interval.

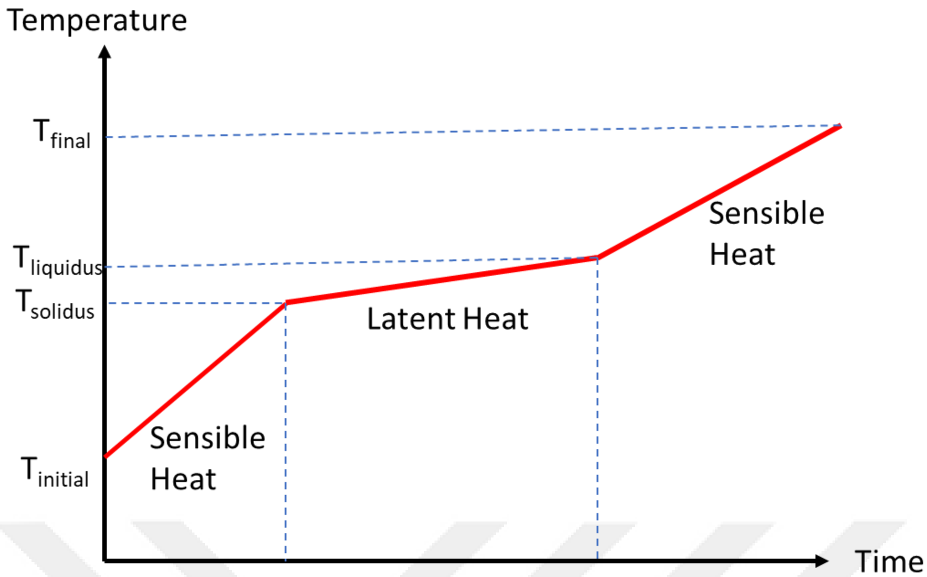

Figure 1.3 Charging Behavior of SL-PCM

PV panels are the great alternative as renewable energy resources. However, the converted energy by the PV panel is low. Moreover, since they work under huge amount of solar irradiation, temperature of the part which converts solar irradiation to the electricity, gets hotter and this semi-conductor loses its conversion ability. SS-PCM is used, in order to provide thermal management to the PV panel. This solid material protects its solid structure while absorbing thermal energy as latent heat. During this latent heat storage in a certain temperature interval, molecular structure of material passes from alpha phase to gamma phase [38].

The structure of this thesis is built on experimental and numerical application. In experimental application, there will be comparison between three different PV panels. Three of them will be checked in terms of their electrical conversion. With the selection of appropriate PV panel, irradiance, ambient temperature, generated power and surface temperature values of that PV panel will be collected. Test results cover only PV panel without use of PCM due to the preparation of the test setup and the difficulty of integration of NPG to the photovoltaic panels. NPG must be melted and poured into a mold to achieve the desired shape and thickness for a photovoltaic panel. However, due to its hardness, the material becomes brittle. After the cooling of neopentyl glycol in the mold, the material changes its shape and have possible curvature. Therefore, surface contact between tedlar of the PV panel and PCM could not be provided enough. Production and assembly of the test setup is not perfect enough to see the benefits of use of SS-PCM on the PV panel. Therefore, performance evaluation of SS-PCM integrated PV panel will be done in the numerical analysis chapter. Moreover, the thermal behavior characterization of the SS-PCM will be shown experimentally. With the guide of the characterization experiment, numerical analysis will be realized. Numerical results will be validated through a commercial analysis software by using experimental data. By applying different thicknesses of SS-PCM to the back surface of the PV panel, the configuration that yields the highest electrical efficiency will be identified.

Improving the performance of the PV panels is worth to examine. Considering the gap in the literature, SS-PCM will be employed in the thesis to slow down the temperature increase of PV panels as an alternative solution. In this context, the objective of the thesis is outlined:

- Enabling thermal management to the PV panels by using SS-PCM's thermal energy storage capacity during daylight
- Thermal characterization of PCM
- Increasing the efficiency of the panel default efficiency
- Comparing the performance of the PV panels with SS-PCM and without SS-PCM
- Studying the ideal PCM thickness for a PV panel

1.4 Thesis Outline

The problem related to the thermal management of PV panels with SS-PCMs has been identified. A literature review on the subject is conducted, and the thesis motivation, problem statement, and thesis objective have been explained based on the findings. To investigate and study the relevant topic, test and experimental studies were carried out, and their results have been shared. In light of the experimental and test results, a parametric study for SS-PCM thickness is conducted. Flowchart of the thesis is presented on Figure 1.4.

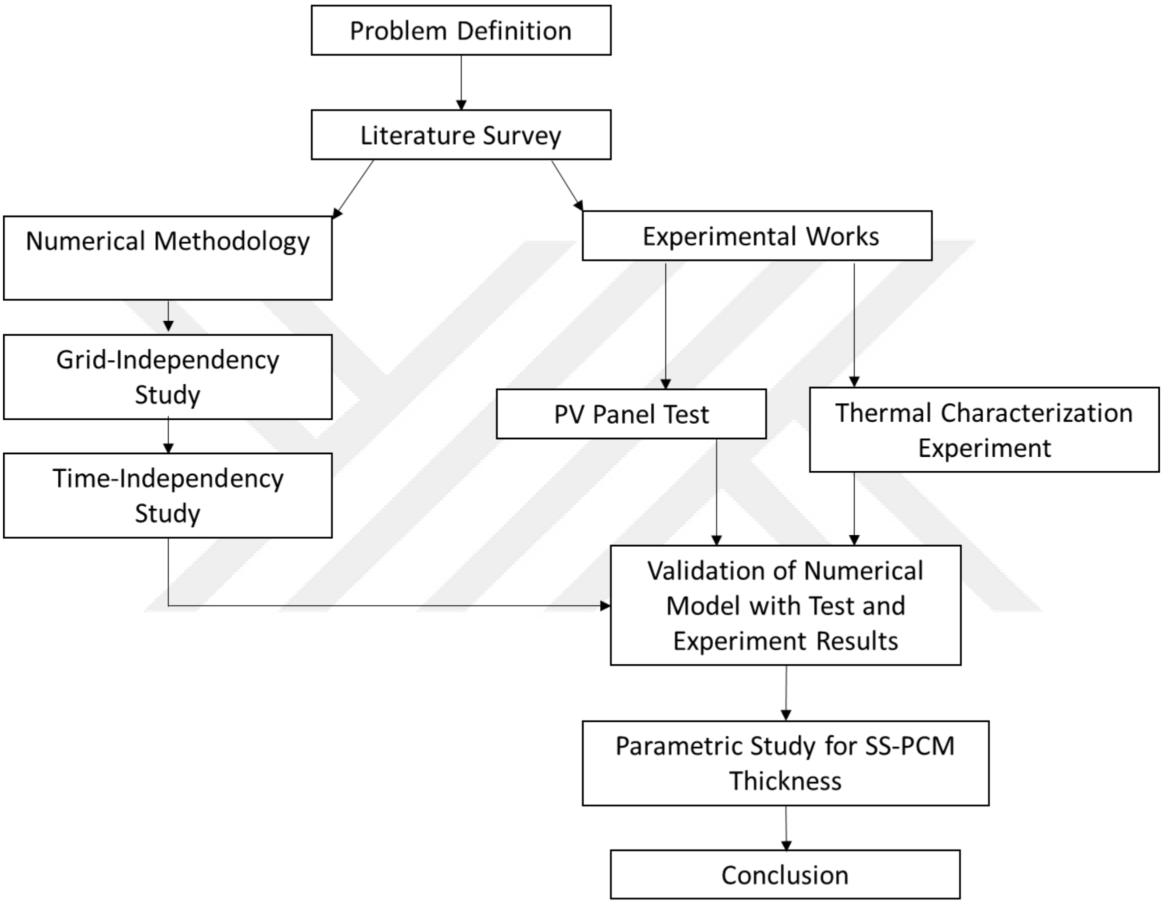

Figure 1.4 Flowchart of the Thesis

CHAPTER 2

METHODOLOGY

2.1 Experimental Work

PV panels are tested to examine their performance and functionality. The collected data from them will be input for the numerical analysis.

A thermal characterization experiment was conducted for the PCM to examine its thermal behavior. The results of this experiment will serve as inputs for the numerical analysis.

The experimental study is divided into two main sections. The first section focuses on testing the PV panel under daylight conditions, while the second section involves the thermal characterization of SS-PCM. The methodology for conducting these experiments is explained. The outputs obtained from the experiments are utilized as inputs and boundary conditions for the numerical analyses.

2.1.1 Photovoltaic Panel Tests

The tests conducted on PV panels to evaluate their performance are described. Moreover, in order to reach ideal thermal management for a PV panel, numerical modelling will be done. The reason why PV panel tests are implemented is gathering data and creating input for the modelling of a PV panel. PV panel modelling will be validated with PV panel test results since PV panel modelling is needed in the SS-PCM integrated PV panel modelling. Data is gathered from the tests to implement them to the numerical analyses as boundary conditions. Performance of PV panel in the tests is compared with numerical results. In this section, PV panel test setup and test procedure are defined.

2.1.1.1 PV Panel Test Setup

PV panel tests were carried out on the roof of the Department of Mechanical Engineering, Middle East Technical University, in August 2024, in order to examine the performance of them.

Test setup includes PV panels, pyranometer, electrical resistances, datalogger, hot wire anemometer and thermocouples. PV panels are used to convert solar energy to electrical energy. Pyranometer is used to measure solar irradiance. Resistances are used as load in front of the panels. Thermocouples are used for that measuring the temperatures on surfaces of panels. Hot wire anemometer is to measure the wind velocity. Datalogger is used to collect the current, voltage and temperature data.

Lexron 12 W Monocrystalline PV panels are used since they have higher power generation capacity than polycrystalline PV panels [41,42]. Their dimensions are 0.355x0.255 mm. Peak power current of the photovoltaic panel is 0.51 Amperes and peak power voltage is 20.70 Volts [42]. Open circuit voltage which is 24.84 Volts.

PV panels work as a power supply and in order to obtain a current flow from the panel, there should be load in front of it. Therefore, aluminum resistances are employed to provide a load to the panels. Current and voltage for maximum power of the PV panel is presented on the datasheet [42]. Peak power current is 0.51 Amperes and peak power voltage is 20.70 Volts. The resistance for peak power is calculated as 40.59 Ohms with Ohm's law. In order to obtain a close value to 40.59, three different aluminum resistances which have 33, 6.8 and 1 Ohms are acquired [43]. 40.8 Ohms serially connected resistances are placed into the test setup. PV panels are presented on Figure 2.1.

Figure 2.1 PV Panels in Test

A pyranometer is used in order to measure the irradiation during the tests. Used pyranometer is Eppley – Model 8-48 [44]. Pyranometer gives voltage data to the data logger. The collected data is converted to the irradiance value by use of a coefficient belongs to the pyranometer. The irradiance collected by pyranometer is applied to the numerical analysis as heat generation for different configurations of PV panel and SS-PCM. Pyranometer and the PV panel is presented in Figure 2.2.

A datalogger is employed in order to measure the voltage, current, irradiance and surface temperatures. The data logger model is Keysight 34972A[45]. Datalogger has 20 channels to collect data and 18 of them to obtain voltage and two of them is for collect current.

A hot-wire anemometer which is Alnor 8570-M is employed to measure the wind velocity during the tests [46]. Wind velocity is measured three times a day. Average of measured wind velocities is used as input in the numerical analysis.

T-type thermocouples are employed in order to measure the surface temperatures on PV panels. T-type thermocouples consist of constantan and copper. The temperature range of them is from -270℃ to 370℃. There are 7 thermocouples on the system. One of them is to measure the ambient temperature. Six of them will be on the photovoltaic panel. Three thermocouples will be on top of the panel. Other three thermocouples will be on the back surface of the panel. Locations of the thermocouples are presented in Figure 2.3.

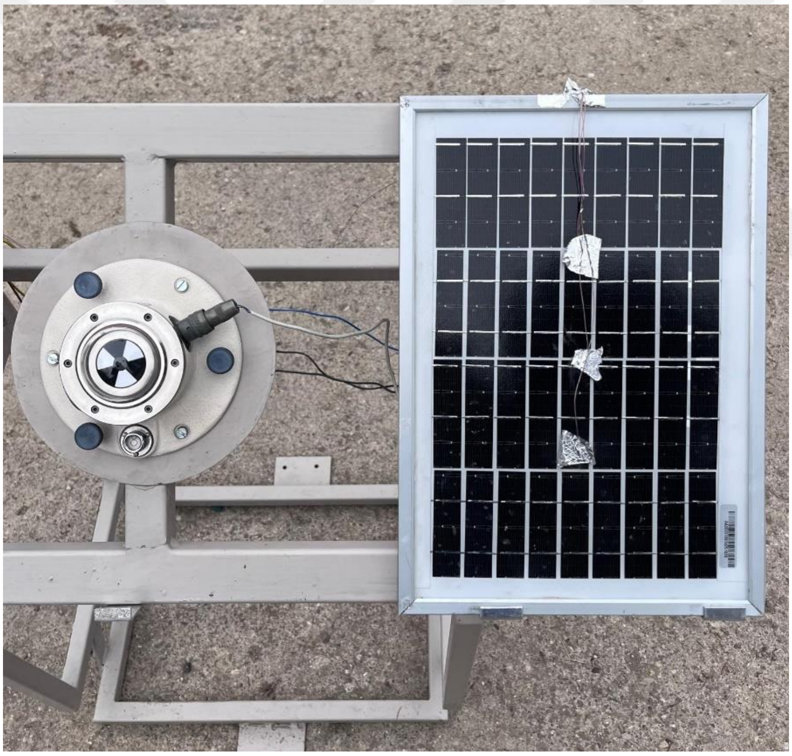

Figure 2.2 Test Setup Including Pyranometer and PV Panel

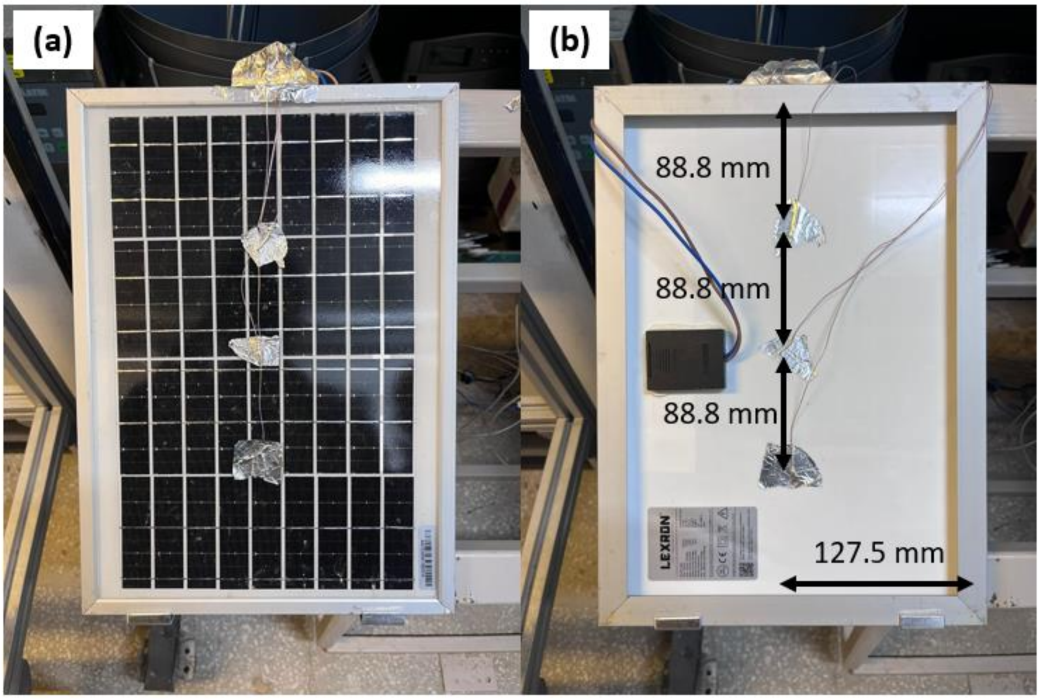

Figure 2.3 Thermocouple Locations on Photovoltaics, **(a)** Top Surface, **(b)** Bottom Surface

Test setup of the thesis is presented in Figure 2.1 and Figure 2.2. Photovoltaic panels are settled on the carcass structure at 33^{o} while looking at the south, with the information on Photovoltaic Geographical Information System [47] in order to obtain the maximum energy. All three PV panels are mounted on the carcass structure as Figure 2.1 to check their compatibility with catalog. For investigation of PV panel and collecting data, a PV panel and a pyranometer are mounted on the carcass structure as on Figure 2.2.

2.1.1.2 PV Panel Test Procedure

Identical three 12 W photovoltaic panels are purchased for PV panel tests since the photovoltaic panels may show different performance characteristics. The open-circuit voltage of the panels is measured to identify the PV panel with performance closest to the catalog specifications. The most similar one to the catalog is used in the daylight test. Photovoltaic panels are presented in Figure 2.1. The ambient temperature is measured as 28.8°C, and the irradiance is measured as 900 W/m². The measurements showed that panel 1 had an open-circuit voltage of 19.21 V, panel 2 had 20.84 V, and panel 3 had 21.14 V. Consequently, panel 3 was selected for the next phase of the test.

The selection of the PV panel to be used enabled the formation of the next test setup. The test setup presented in Figure 2.2. PV panel and pyranometer on the same carcass structure are settled on the roof of the mechanical engineering department in August. The tests are conducted for several days in order to provide consistency between the data since the atmospheric circumstances may be different for every day. One of the days which have smooth data is chosen as the sample and input. During the tests, irradiance, photovoltaic panel temperatures, ambient temperature and wind velocity are collected.

Numerical model of PV panel will be validated by using test outputs. Irradiance, ambient temperature and wind velocity are applied as boundary conditions. Temperatures values measured from PV panel are used for comparison with numerical results. The test outputs will be guide for finding suitable thermal management solution and maximizing generated electricity of photovoltaic panels.

2.1.2 Thermal Characterization Experiment of SS-PCM

An experimental setup is established to investigate the thermal behavior of NPG. Target of this study is that showing the characterization of the NPG and validity of the literature information. Moreover, another purpose of conducting this experiment is to provide a reference for numerical modeling of NPG. The created numerical model for NPG will be validated with the results of thermal characterization experiment. The outputs of this study are used as input in the numerical modelling of SS-PCM.

2.1.2.1 Thermal Characterization Experimental Setup

Experimental setup includes a base, a silicon heater, an aluminum casing, neopentyl glycol, a power source, thermocouples and a data logger. Another device which is Comark C9008 also used to measure temperatures in this experiment [48]. The measurements of that device are checked with measuring the locations which are measured by other thermocouples. Material properties of the aluminum is indicated in Table 2.1. Except power source, the other components are already explained. Used power source is Keysight 8761A [49]. It can provide maximum power 5100 W with 300 V and 17 A. Experimental setup is presented in Figure 2.4. Moreover, to find the emissivity of the aluminum Optris PI400i thermal camera is used [50].

Table 2.1 Aluminum thermophysical properties

Property	**Value**
$\rho\ (kg/m^3)$	2701 [51]
$c_p\ (kJ/kgK)$	0.902 [51]
$k\ (W/mK)$	190 [51]
ε	0.2

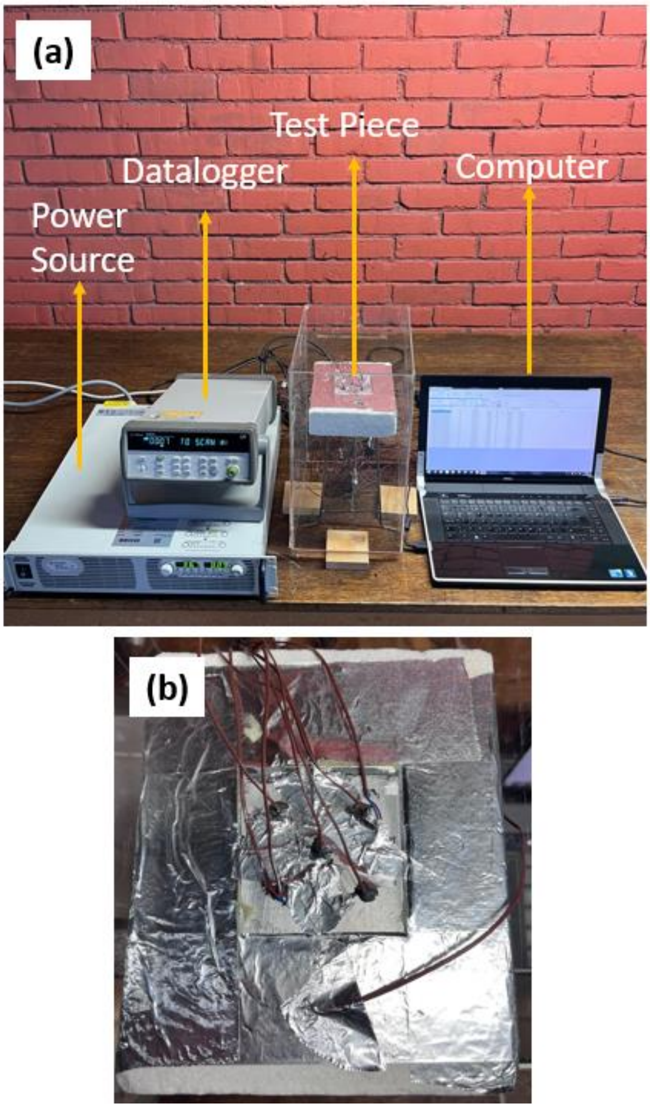

Figure 2.4 **(a)** Experimental Setup, **(b)** Top Surface of Experiment Test Piece

Aluminum casing filled with NPG is presented in Figure 2.5. Melted NPG is poured down into the casing. After its cooling, the excess material on the seen surface is removed. The gap left for material filling is sealed using an aluminum sheet of identical thickness.

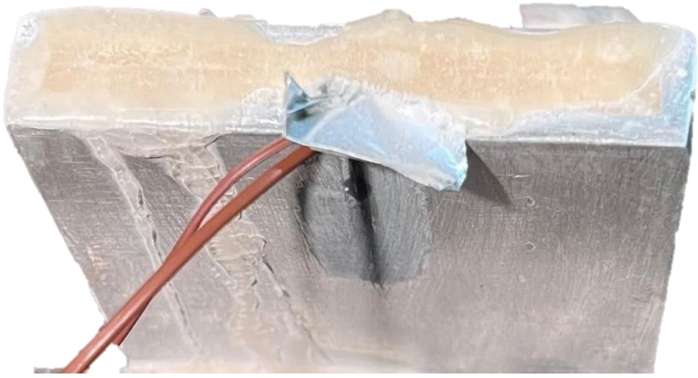

Figure 2.5 Aluminum Casing Filled with NPG

A silicon heater and aluminum casing filled with NPG is embedded into a base material which is ceramic wool. Aluminum casing is filled with NPG, since shaping the PCM is challenging in the laboratory circumstances. When the heat is transferred to the aluminum directly, there will be no contact resistance between aluminum and PCM. Exploded view of experimental setup and thermocouple locations are presented on Figure 2.6. Coordinates of thermocouple locations are represented on Table 2.2.

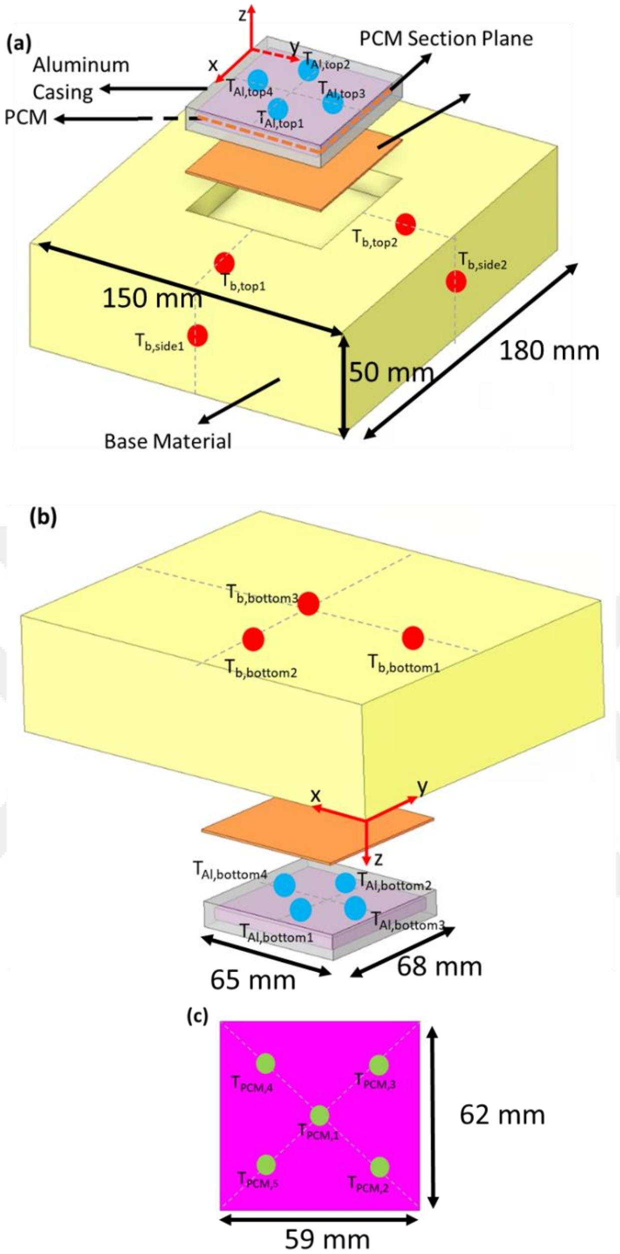

Figure 2.6 Exploded Schematic View and Thermocouple **(a)** Isometric View, **(b)** Bottom of View, **(c)** Inside of PCM

Table 2.2 Coordinates of Thermocouple Locations

	x (mm)	**y** (mm)	**z** (mm)
$T_{Al,top1}$	124	75	0
$T_{Al,top2}$	56	75	0
$T_{Al,top3}$	90	107.5	0
$T_{Al,top4}$	90	42.5	0
$T_{b,top1}$	152	75	0
$T_{b,top2}$	90	128.75	0
$T_{PCM,1}$	90	75	-6.5
$T_{PCM,2}$	105.5	89.75	-6.5
$T_{PCM,3}$	74.5	89.75	-6.5
$T_{PCM,4}$	74.5	60.25	-6.5
$T_{PCM,5}$	105.5	60.25	-6.5
$T_{Al,bottom1}$	124	75	-11
$T_{Al,bottom2}$	56	75	-11
$T_{Al,bottom3}$	90	107.5	-11
$T_{Al,bottom4}$	90	42.5	-11
$T_{b,bottom1}$	90	37.5	-50
$T_{b,bottom2}$	45	75	-50
$T_{b,bottom3}$	90	75	-50

Temperatures are measured from eighteen different locations. Four of them is between silicon heater and aluminum casing, five of them are settled in the middle of the solid-solid phase change material, four of them are on top of the aluminum casing, three of them are under the base material, one of them is on the width axis side of base material, one of them is on the length axis side of the base material and two of them is on the base material at different locations. If there are several thermocouples on a surface, average value of them is used for calculations. Since the experimental setup is symmetric, for the surfaces which do not have thermocouple on it, counterpart thermocouple readings are used for calculations. Thermocouple locations are presented in Figure 2.6. Red dots are for the measurement location on the base material. Blue dots are for the measurement location on the aluminum. Green dots are for the measurement inside PCM. T_b is for base material. T_{Al} is for aluminum temperatures. T_{PCM} is for PCM temperatures. The blue dashed lines are located to show the regions which will be used to calculate heat transfer to the surroundings.

2.1.2.2 Thermal Characterization Experimental Procedure

Target of this experiment is the thermal characterization of NPG. Latent heat absorption behavior will be observed. Thermal conductivity will be calculated with the collected data. In order to reach the desired aim of the experiment, constant 3.5 W power is supplied to the system until the system reaches steady state. When temperature values reach the steady state, collected temperature data will be covering the latent heat behavior and be enough to calculate thermal conductivity of NPG. Furthermore, the emissivity of the top surface of the aluminum casing will be obtained by using the thermal camera. Thermal camera offers the opportunity to acquire the emissivity iteratively, if the surface temperature is known. Thermal camera measures the surface temperature by using an embedded emissivity value. A known surface temperature value was achieved by modifying the emissivity value iteratively. Infrared image of experimental setup is represented in Figure 2.7. Emissivity of aluminum top surface is obtained as 0.2. Experimental setup which includes also power supply, datalogger and computer is presented in Figure 2.4.

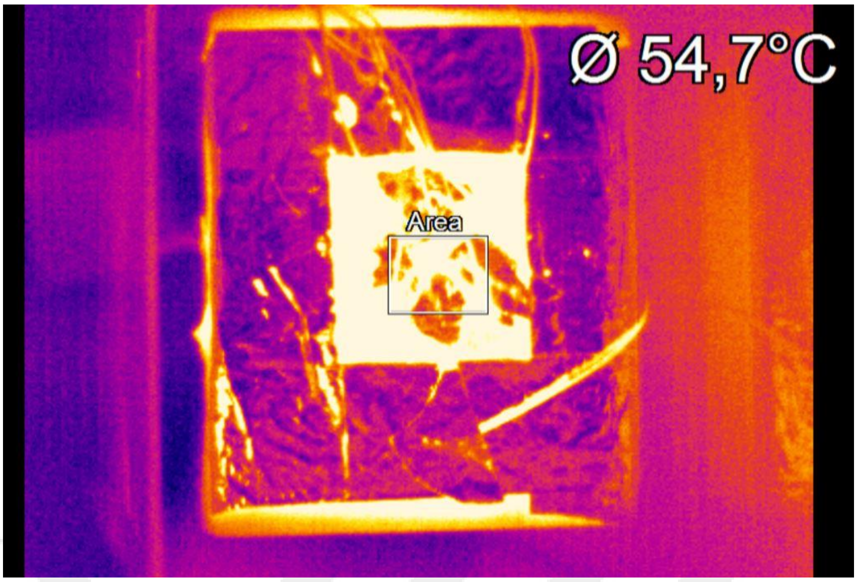

Figure 2.7 Aluminum Casing Top Surface Temp. Measurement (Infrared Image)

Calculation of thermal conductivity is one of the concerns in this test. There are several different values for thermal conductivity values in literature. Thermal conductivity of NPG is mostly 0.24 W/mK [36] and there are several values between 0.15-0.42 W/mK [37] in the literature. Therefore, calculating the thermal conductivity of NPG is preferred. Thermal conductivity of the neopentyl glycol is calculated by using one-dimensional thermal circuit. Casing has 11 mm thickness 68 mm length and 65 mm width. Heater below of the casing has similar dimension. Moreover, all around the casing is covered with a material which has low thermal conductivity. Therefore, one dimensional conduction is assumed through casing. Thermal circuit is created between bottom of aluminum casing and top of aluminum casing since the casing has 11 mm thickness. The scheme in Figure 2.8 is created for every layer of the aluminum casing.

Figure 2.8 Thermal Circuit of the Experimental Setup in Steady-State

Heat transfer equations covering Figure 2.8 is denoted on Eqns. 2.1 – 2.5.

$$R_{Al,1} = \frac{L_{Al}}{k_{Al} x A} \qquad (2.1)$$

$$R_{PCM} = \frac{L_{PCM}}{k_{PCM} x A} \qquad (2.2)$$

$$R_{Al,2} = \frac{L_{Al}}{k_{Al} x A} \qquad (2.3)$$

$$R_{total} = R_{Al,1} + R_{PCM} + R_{Al,2} \qquad (2.4)$$

$$q = \frac{T_{Al,bottom} - T_{Al,top}}{R_{total}} \qquad (2.5)$$

In this experiment, a constant power input will be applied until the system reaches a steady state. The experiment will be conducted twice to verify repeatability. Using the temperature data collected from thermocouples, the energy balance of the system will be calculated under steady-state conditions. Surface temperatures all around the experiment box are used in order to implement this process. Surface temperatures are employed while calculating the free convection around the test setup. Additionally, the top surface temperature of aluminum is used to calculate the energy loss by radiation from it. For top surface, upper surface of hot plate Nusselt number correlation in Eqn. 2.6; for bottom surface, lower surface of hot plate Nusselt number correlation in Eqn. 2.7 and for side surfaces vertical plate Nusselt number correlation in Eqn. 2.8 is applied respectively [52].

$$Nu = 0.54 Ra_L^{0.25} \qquad 10^4 \leq Ra_L \leq 10^7, Pr \geq 0.7 \qquad (2.6)$$

$$Nu = 0.52 Ra_L^{0.2} \qquad 10^4 \leq Ra_L \leq 10^9, Pr \geq 0.7 \qquad (2.7)$$

$$Nu = 0.68 + \frac{0.67 * Ra_L^{1/4}}{[1 + \left(\frac{0.492}{\mathrm{Pr}}\right)^{\frac{9}{16}}]^{\frac{4}{9}}} \qquad Ra_L \leq 10^9 \qquad (2.8)$$

Rayleigh number, Nusselt number, radiative heat transfer and Newton’s law of cooling is denoted in Eqns. 2.9-2.12.

$$Ra_L = \frac{g\beta(T_s - T_\infty)L^3}{\nu\alpha} \qquad (2.9)$$

$$Nu = \frac{hL}{k} \tag{2.10}$$

$$q_{rad} = \varepsilon A \sigma (T_s^4 - T_\infty^4) \tag{2.11}$$

$$q = hA(T_s - T_\infty) \tag{2.12}$$

Energy balance is established with the data collected from experiment. Heat flux passing through the aluminum casing is calculated. The thermal resistance between top surface and bottom surface is computed. Thermal conductivity of the NPG is determined from thermal resistance of itself as Eqn. 2.2 since thermal resistances of aluminum layers are known.

Thermal characterization of NPG is done by applying this experimental work. Thermal behavior of NPG is shown during latent heat absorption and thermal conductivity of it is calculated.

2.2 Numerical Study

The numerical studies conducted for the investigation is described in this section. Numerical model done for PV panel test and thermal characterization experiment are validated by test and experiment results since SS-PCM integrated PV modelling includes both modelling methods in it.

Numerical studies are divided into three parts. The PV panel test and thermal characterization experiment are modeled numerically. The modelling of those validation is guiding for the final numerical analyses. Computational domains, governing equations, and boundary conditions are defined, and grid independence and time independence analyses are performed.

2.2.1 Numerical Model for PV Panel Test

The layers of the PV panel are modelled in this numerical study. The data obtained from the PV panel test is used as input and boundary condition for the numerical study. Numerical model validation is realized to ensure the modelling of PV panel is accurate. Inputs of the numerical study are irradiance, ambient temperature and wind velocity. Before the validations, grid independency and time step independency study are performed. Validation of PV panel test is realized to use the PV panel modelling in SS-PCM integrated PV panel analyses. Computational domain, governing equations and boundary conditions for a PV panel will be common in both analyses modelling.

2.2.1.1 Computational Domain

The computational domain of PV panel is depicted in Figure 2.9.

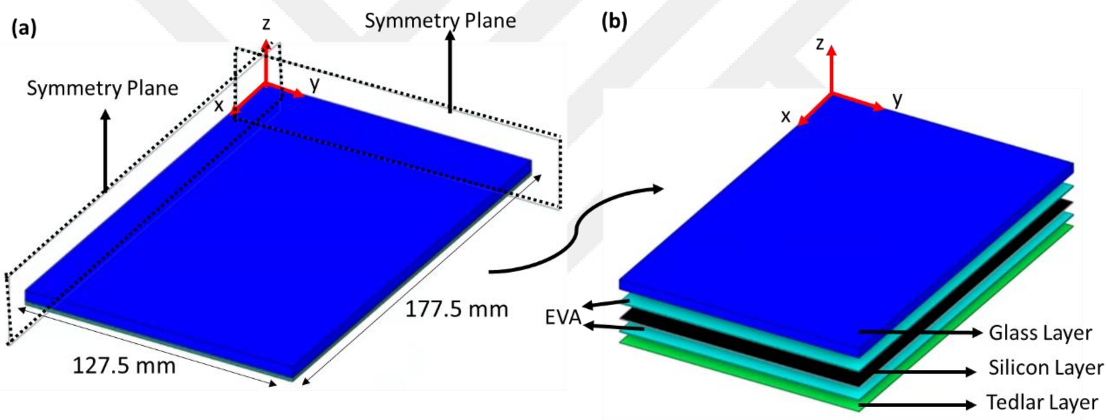

Figure 2.9 **(a)** Computational Domain, **(b)** Exploded View

Computational domain consists of five layers of a PV panel [4]. They are glass, ethylene-vinyl-acetate (EVA), silicon and tedlar. Materials and their properties are presented in Table 2.3.

Table 2.3 Material Properties of Layers of Photovoltaic Panel [53]

Materials	**c_p** (kJ/kgK)	**ρ** (kg/m^3)	**k** (W/mK)	**Thickness (mm)**
Glass	0.5	3000	1.8	$d_g = 4$
EVA	2.09	960	0.35	$d_e = 0.5$
Silicon	0.677	2330	148	$d_s = 0.3$
Tedlar	1.25	1200	0.2	$d_t = 0.1$

The computational domain includes the layers of a PV panel. Since the PV panel has a symmetrical geometry, quarter of the PV panel is used domain. Symmetry planes are located on $x = 0$ and $y = 0$.

2.2.1.2 Governing Equations

In the numerical solution of the PV panel, a conduction modelling is done with following assumptions:

- Transient solution is applied.
- The thermophysical properties of the materials are constant.
- Collected irradiation, ambient temperature and wind velocity data are given as input.

The governing equations for transient conduction of a PV panel is denoted by Eqn. 2.13. In Eqn. 2.13, T stands for temperature, $\dot{q}$ stands for volumetric heat generation, t stands for time. k and α are thermal conductivity and thermal diffusivity.

$$\frac{\partial^2 T}{\partial x^2} + \frac{\partial^2 T}{\partial y^2} + \frac{\partial^2 T}{\partial z^2} + \frac{\dot{q}}{k} = \frac{1}{\alpha}\frac{\partial T}{\partial t} \quad (2.13)$$

The heat source which will be used as irradiance in the numerical analysis is denoted on Eqns. 2.14-2.18 [4,28].

$$I_{PV} = (\tau\alpha)_{eff} * I_{ir} \quad (2.14)$$

$$S = I_{pv} - \eta_c * I_{ir} \quad (2.15)$$

$$\eta_c = \eta_{ref}[1 - \beta_{ref}(T - T_{ref})] \quad (2.16)$$

$$\eta_{ref} = \frac{P_{max}}{I_{ir}} \quad (2.17)$$

$$\beta_{ref} = \frac{1}{T_0 - T_{ref}} \quad (2.18)$$

The generated heat at the silicon layer of the PV panel is modelled as in Eqn 2.15 to calculate operating temperature of it. Solar irradiance is applied as transmitted and absorbed radiation to the PV panel. Effective transmissivity and absorption value is 0.905 [54]. The difference between total amount of irradiance and the irradiance converted to the electricity is converted heat. The irradiance converted to electricity is obtained with cell conversion efficiency. Cell conversion efficiency, η_c, changes with respect to operating temperature of PV panel as denoted in Eqn. 2.16. Moreover, it needs reference efficiency and temperature coefficient of PV panel. Reference efficiency, η_{ref}, is acquired with maximum power generation. Temperature coefficient of the PV panel is β_{ref} in Eqn. 2.18. The temperature which causes the drop of efficiency of a PV panel to zero is T_0 in Eqn. 2.18. This temperature is equal to 270°C for crystalline cells and β_{ref} is equal to 0.004 [55].

The governing equations are solved by Ansys FLUENT which is using finite volume method [40]. The energy equation employed the second order upwind scheme to solve the problem. The Eqns. 2.14-2.18 are utilized to model the PV panel in software.

2.2.1.3 Boundary Conditions

Silicon layer is where energy conversion takes place. Heat source will be defined into the silicon layer as volumetric heat source with the Eqn. 2.19 [4] since top surface of glass layer is used to define convective heat transfer and emitted radiative heat transfer. In Eqn. 2.19, d_s is the thickness of the silicon layer.

$$\dot{q} = \frac{S}{d_s} \tag{2.19}$$

There are two boundary conditions which are convective and radiation on top of the PV panel surface at $z = 0$. Convective heat transfer coefficient is applied as input which is denoted on Eqn. 2.20 and V_w is wind velocity. Eqn. 2.20 was derived from an experimental study by Sharples et al. [56]. In that study, the convection coefficient of a PV panel surface is investigated on a roof of a building experimentally.

$$h_{top} = 2.6\,V_w + 7.9 \tag{2.20}$$

Radiation heat transfer equation is used for radiative emission on top surface of the photovoltaic panel. Radiation heat transfer equation is denoted on Eqn. 2.21. Surface temperature of PV panel in the test is applied as initial temperature for domain. Emissivity of the glass top surface is ε and it is equal to 0.91 [57]. The Stefan-Boltzmann constant is shown with σ. Temperature of the sky is T_{sky} and its value is calculated by Eqn. 2.22 [30]. Ambient temperature is T_{amb}.

$$q_{rad}" = \varepsilon\sigma(T_{top}^4 - T_{sky}^4) \tag{2.21}$$

$$T_{sky} = 0.0375{T_{amb}}^{1.5} + 0.32T_{amb} \tag{2.22}$$

On the side walls, where $x = 177.5\,mm$ and $y = 127.5\,mm$; and the bottom surface of the photovoltaic panels where $z = -5.4\,mm$, convective heat transfer coefficient is assumed as 7 W/m^2K [4].

2.2.1.4 Grid Independence Study

A numerical model is created, in order to do the modelling of the PV panel. Grid independence study is applied to make the results not changing with different element numbers. It provides efficient use of computational resources. Three different grid sizes which are 100, 200, 400 and 2.5K cell numbered models are compared. A transient thermal analysis applied and the results of that analysis is presented on Figure 2.10.

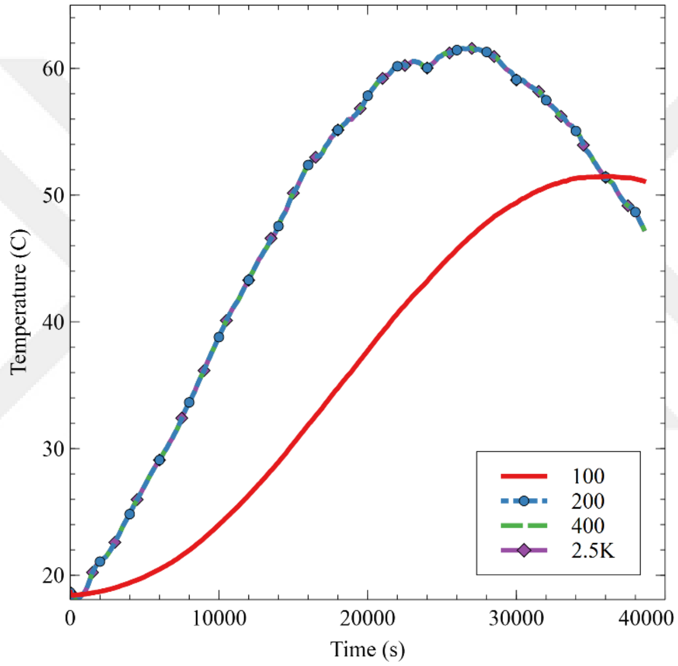

Figure 2.10 Glass Top Surface Temperatures for Different Element Numbers

The results have compatibility between each other as represented in Figure 2.10. 100 cell number solution gives much different results than the others. Except 100 cell number, other ones are suitable for the next analyses. However, 2.5K cell number is selected for the next steps since the analyses which includes SS-PCMs requires more cell number in order to provide cell size compatibility. As a result, the grid which has 2.5K cells is selected mesh for the next analysis. Therefore, it was reached that the model of the photovoltaic panel is grid independent. Grid model is presented on Figure 2.11. Since model contains simple conduction and geometry is rectangular, hexahedral cell type is preferred. The cells can follow the geometry completely.

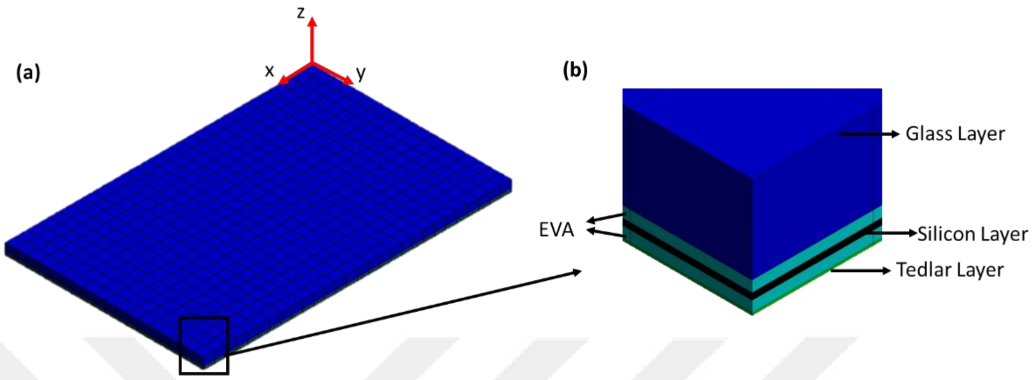

Figure 2.11 **(a)** PV Panel Computational Domain Mesh Structure, **(b)** Detailed View

2.2.1.5 Time Step Independence Study

The numerical analysis will give a solution depending on time since the analysis is transient. The time step independence study is applied to make the results not changing with different time steps and minimize the solution time. A time independence study should be done for the definite solution. Different time steps which are 40s, 320s, 640s, 1280s, 2560s and 5120s are compared. PV panel top center temperature is evaluated.

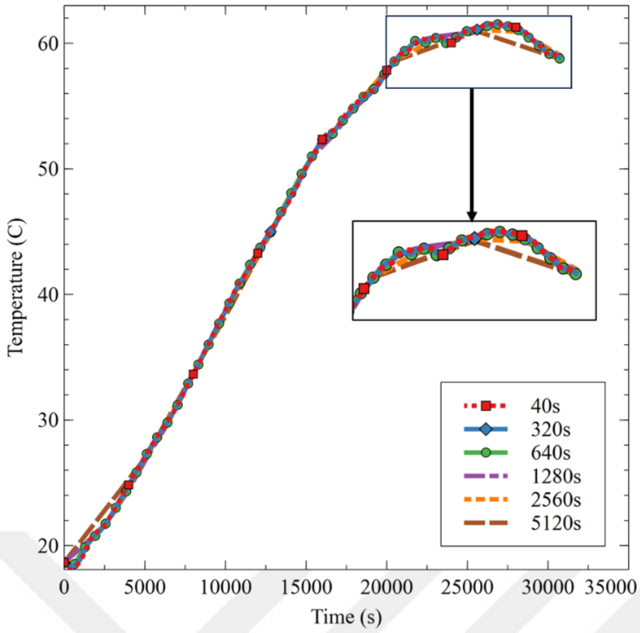

Figure 2.12 Glass Layer Top Surface Temperatures for Different Time Steps

All three results of 640s, 320s and 40s are following the close path as presented in Figure 2.12. 1280s, 2560s and 5120s results become a different than the others while approaching to the end. It may be said that the numerical model is time independent. However, 40s time step is selected for the next analyses due to suitability with time steps of collected data and resolution of results.

2.2.2 Numerical Investigation for Thermal Characterization of SS-PCM

Numerical investigation of thermal characterization is done for the validation of numerical model for SS-PCM since SS-PCM integrated PV panel modelling includes SS-PCM. Since numerical modelling of SS-PCM is critical, modelling of it is validated with experimental results in this section. Validation of applied model for SS-PCM will be used in SS-PCM integrated PV modelling and it will guide to reach ideal SS-PCM thickness in the final numerical analyses.

2.2.2.1 Computational Domain

A thermal characterization experiment is conducted to see the latent heat absorption of the PCM and reach the thermal conductivity of it. The PCM filled aluminum casing is the domain of the numerical analysis.

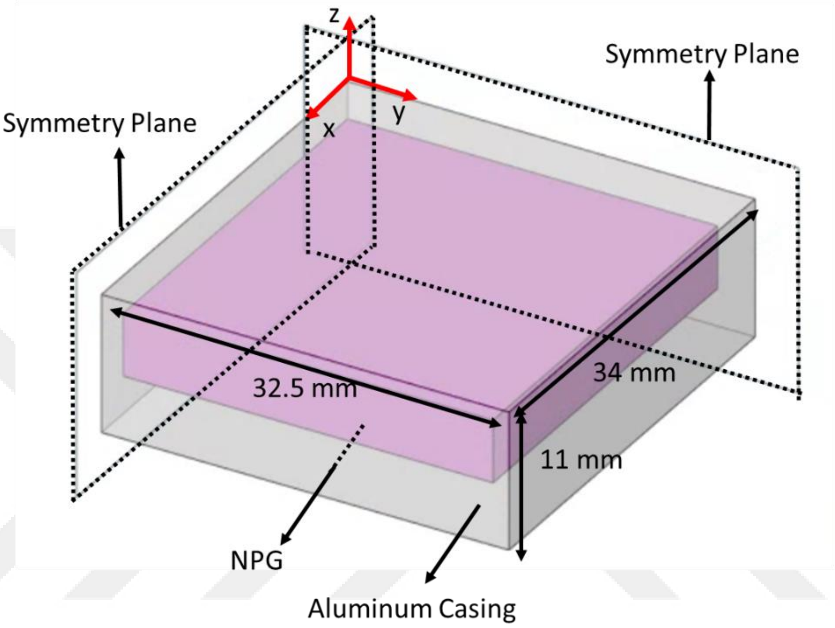

Figure 2.13 Computational Domain of Characterization of PCM

Numerical domain is illustrated in Figure 2.13. The modelling is done for the quarter of the characterization experiment setup since the geometry is symmetric. $x = 0$ and $y = 0$ planes are the symmetry planes. The thermophysical properties of NPG and aluminum are shown in Table 1.1 and Table 2.1.

2.2.2.2 Governing Equations

In this section of the thesis following assumptions are made for numerical analysis:

- Analysis is transient.

- Thermophysical properties of the materials are constant. Thermal conductivity of PCM is used as obtained from the experiment.
- Time dependent power is applied to the system.

The equation which is responsible for the solution of the problem domain is transient heat conduction equation. Transient heat conduction equation is denoted on Eqn. 2.13.

The critical modeling pertains to SS-PCM, as its performance is evaluated in the thesis. When the SS-PCM reaches a certain temperature, the PCM begins to absorb heat as latent heat. However, the SS-PCM maintains its solid structure, meaning that its heat transfer and phase change processes are solely governed by conduction. Therefore, the governing functions of modelling the SS-PCM is based on enthalpy method [58]. Although SS-PCM retains its solid phase after phase transitions and it induces internal energy change, the modelling of this transition is defined as enthalpy method in the literature. The conduction taking place in the system is solved by using ANSYS Fluent [40]. The governing equations which belong the enthalpy method are denoted on Eqns. 2.23-2.25.

$$\beta = \begin{cases} 0, & T < T_{pc1} \\ 1, & T_{pc2} < T \\ \frac{T-T_{pc1}}{T_{pc2}-T_{pc1}}, & T_{pc1} < T < T_{pc2} \end{cases} \tag{2.23}$$

$$H = (H_{ref} + \int_{T_{ref}}^{T} c_p dT) + \beta L \tag{2.24}$$

$$H = h + \Delta H \tag{2.25}$$

Phase change fraction of the SS-PCM is denoted on Eqn. 2.23 and phase change fraction is β. Temperature of the material is T. Starting temperature of the phase change is T_{pc1}. Final temperature of the phase change is T_{pc2}. When the material temperature is below the phase change initiation temperature, β is 0. Conversely, when the temperature exceeds the phase change completion temperature, β is 1. For temperatures between the initiation and completion points, β is calculated using the ratio defined in Equation 2.23. Eqn. 2.24 stands for the enthalpy value of the material depending on phase change fraction of the material. It may be simplified as on Eqn. 2.25 [59]. ΔH is equal to βL and this term gives the enthalpy change depending on phase change fraction where L is latent heat. The conservation of energy equation of the system is denoted on Eqn. 2.13. Enthalpy is H, density is ρ and thermal conductivity is k. The momentum equation is not required for this problem domain, since the SS-PCM remains in its solid phase.

2.2.2.3 Boundary Conditions

Temperature outputs of thermal characterization experiment are used in order to validate the model for phase change material. Computational domain of created model is depicted in Figure 2.13.

Symmetry boundaries located at $x = 0$ and $y = 0$ are depicted in Figure 2.13. Aluminum side walls are insulated at $x = 34\ mm$ and $y = 32.5\ mm$. As heat source, heat flux is applied from bottom of casing at $z = -11\ mm$. To reach time dependent heat flux, the heat flux value released from the top surface of the aluminum casing at $z = 0\ mm$ and stored energy by NPG as sensible heat are summed up until phase change. During the phase change, the heat released from the top surface of the aluminum casing and the latent heat of NPG are combined. After the phase change, the heat released from the top surface of the aluminum casing and the sensible heat of NPG are summed and applied as heat flux in the time domain for specific time steps. There are convective and radiative boundary condition on top surface of the aluminum casing at $z = 0\ mm$. Convection constant which is calculated from the experiment used as boundary condition. Moreover, by using the emissivity reached on thermal camera, radiation boundary condition is defined to the top surface of aluminum. Other side walls are assumed as isolated.

2.2.2.4 Grid Independence Study

Modelling of SS-PCM has critical role in modelling of SS-PCM integrated PV panel. Therefore, numerical model of thermal characterization experiment will be validated with results of the experiment. Grid independence study is done in order to make the model have results not changing with different element numbers. Temperature data taken from top surface of aluminum is compared with the calculation of relative errors. Top surface temperatures of aluminum with respect to different cell numbers are indicated on Figure 2.14. The analysis which has 2.5K cell number does not give logical results. The analyses which have 5K cells and 10K cells validate each other. They have pretty close solutions. Numerical analysis yielded highly consistent results. Relative error between 5K cell and 10K cell is 0.14 %.

As a result, the solution does not change with different cell sizes after 5K cell number. It may be said that the investigation become mesh independent. In order to reduce the solution time, the study will continue with the lowest cell number.

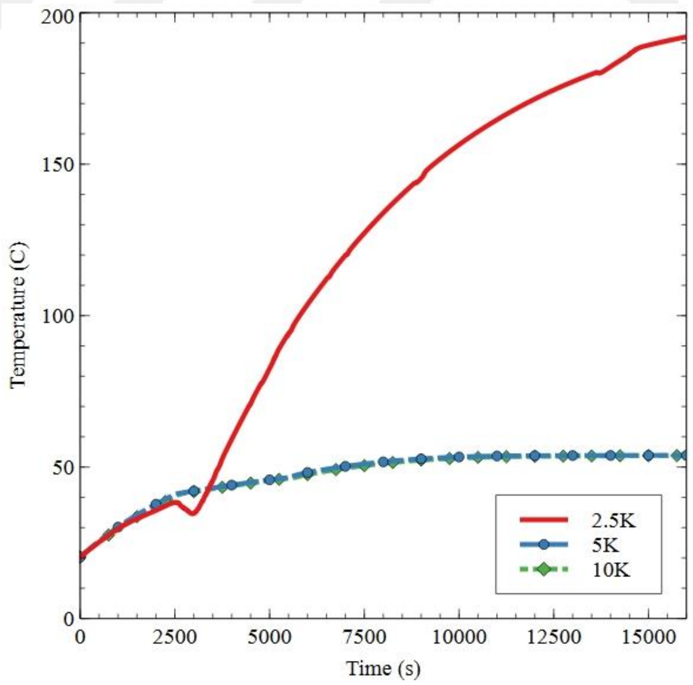

Figure 2.14 Aluminum Top Surface Temperature for Different Element Numbers

Computational domain mesh structure of the study is represented on Figure 2.15. Since model contains simple conduction and geometry is rectangular, hexahedral cell type is preferred. The cells can follow the geometry completely.

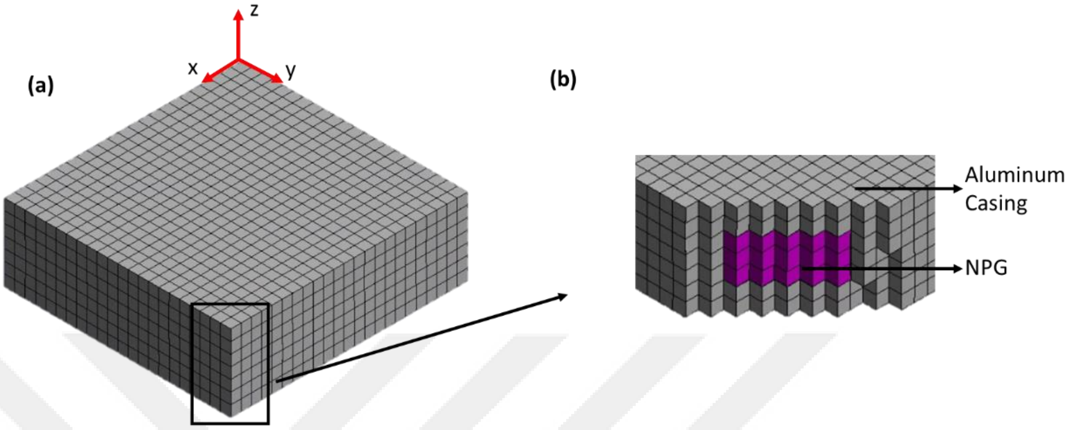

Figure 2.15 **(a)** Computational Domain Mesh Structure, **(b)** Detailed View

2.2.2.5 Time Step Independence Study

Thermal characterization of PCM experiment is modelled to validate SS-PCM model. Results for different time step sizes are compared to make the model have results not altering with different time steps and accurate solutions with short solution time. The data taken from top surface of aluminum is used. Results of the study is presented in Figure 2.16.

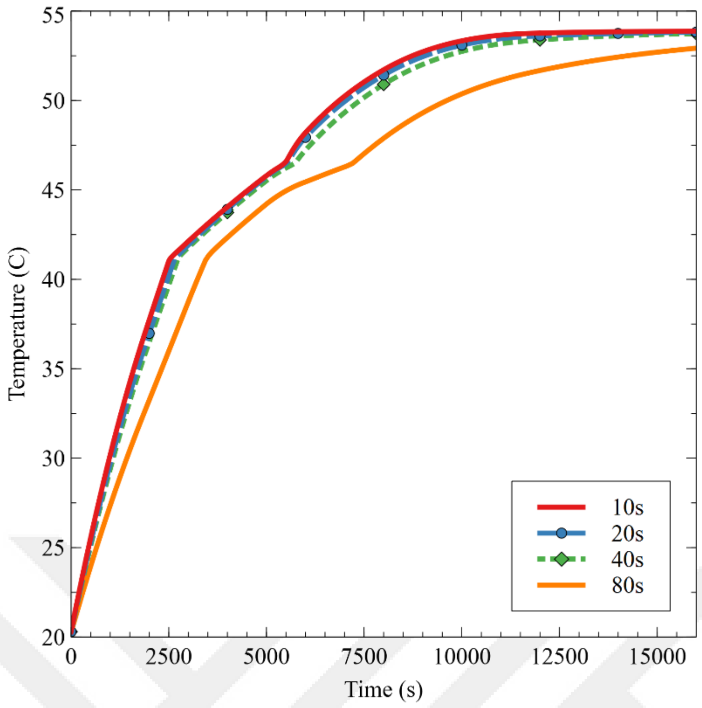

Figure 2.16 Aluminum Top Surface Temperature for Different Time Steps

The error between 10s time step and 20s time step is 0.53% and between 20s time step and 40s time step is 0.85% at 8800th second. Time step independence investigations represented highly consistent results. Therefore, it may be said that the solution becomes time independent.

2.2.3 Numerical Study of SS-PCM Integrated PV Panel

Numerical study of SS-PCM integrated PV panel is done to show decreasing operating temperature and increasing cell conversion efficiency of PV panel. Different PCM thicknesses are modelled with a PV panel to have an ideal thermal management solution for a PV panel. Numerical models of PV panel and SS-PCM done in the previous sections are combined to have SS-PCM integrated PV panel.

SS-PCM integrated PV panel covers the domain, equations and boundary conditions of previous sections, it contains both PV panel and PCM together. Therefore, modeling of them will be combined. Grid independency and time independency study are done for the final model.

2.2.3.1 Computational Domain

Numerical analysis is done to identify the ideal design for the thermal management of SS-PCM integrated PV panel. The physical model of the PV panels has the same dimensions as in the test setup. It is assumed that SS-PCM has perfect contact with the PV panel depicted in Figure 2.9. The PV panel has 255 mm width and 355 mm in length. Exploded view of the domain is presented in Figure 2.17. SS-PCM, materials of the panel layers and their thermophysical properties are represented in Table 1.1 and Table 2.3.

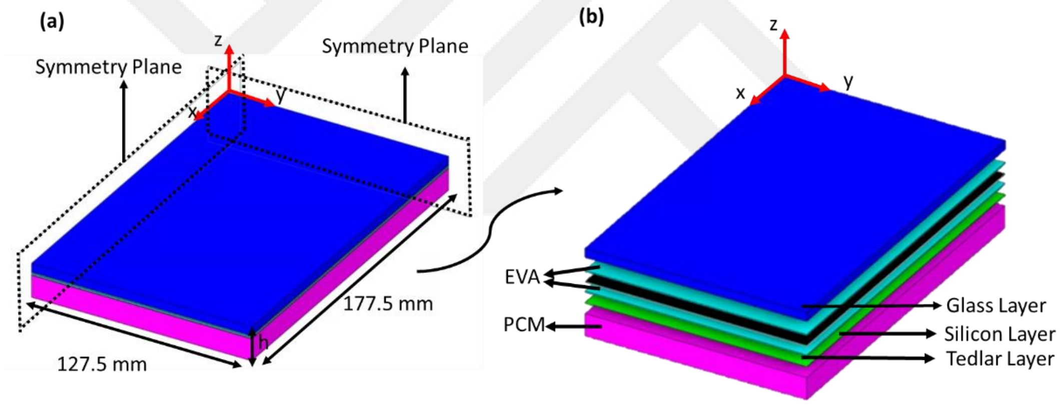

Figure 2.17 **(a)** Computational Domain, **(b)** Exploded View

The domain consists of quarter of the geometry due to symmetry on $x = 0, y = 0$ planes in the simulations. Different SS-PCM thickness values will be used. 10 mm, 20 mm, 30 mm, 40 mm, 50 mm and 60 mm thickness values will be analyzed numerically, since Ahmad, A. et al. [4] used around those thickness values for solid-liquid phase change material.

2.2.3.2 Governing Equations

SS-PCM integrated PV panel numerical analyses are implemented with following assumptions are made for numerical analysis:

- Analysis is transient.
- Thermophysical properties of the materials is constant. Thermal conductivity of PCM is used as obtained from the experiment.
- Collected irradiance, ambient temperature and wind velocity data are the inputs of the analysis.

Governing equations are defined for PV panel and SS-PCM. This part of the thesis covers both parts of the equations since the system includes PV panel and PCM together. The energy equation employed the second-order upwind scheme to solve the problem. PCM keeps its solid phase, the momentum equation is not needed in this problem domain.

2.2.3.3 Boundary Conditions

Computational domain is illustrated in Figure 2.17. The system has SS-PCM integrated PV Panel. In this numerical domain, the silicon part of the PV will have volumetric heat generation. Top surface of the PV panel at $z = 0$ will have radiation emission and Sharples et al. [56]'s convection coefficient. Convection coefficient associated with the other sides of the PV at $x = 177.5\ mm$ and $y = 127.5\ mm$ and bottom of the PCM at $z = -h$ is $7\ W/m^2K$. Symmetry boundaries of the computational domain are modelled at $x = 0$ and $y = 0$ planes. In this study, test data which are irradiance, ambient temperature and wind velocity will be used as input.

2.2.3.4 Grid Independence Study

Three different analyses are applied in order to implement grid independency study. The starting grid number is 950, and the last grid number is 30K. In order to evaluate the mesh numbers, efficiency data of PV panels with PCM is collected from the analysis. The collected data is presented in Figure 2.18. All three analysis show similar trends under irradiance input. In order to evaluate the mesh independency study, relative approximate errors are calculated. The minimum efficiency values are selected since minimum efficiency values seem almost on the same time step, in order to obtain relative error of the data.

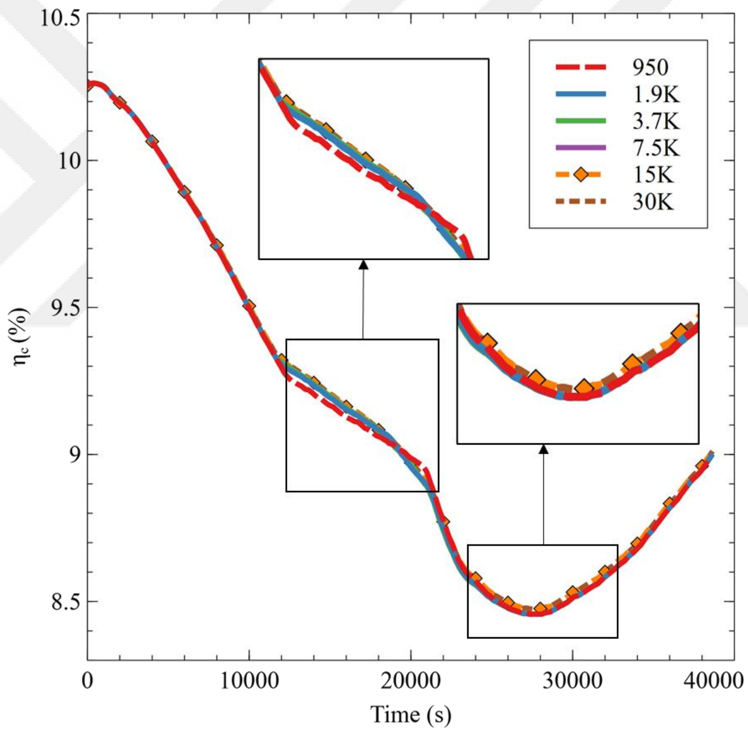

Figure 2.18 Cell Conversion Efficiency for Different Element Numbers

The results of 950, 1.9K and 3.7K cell numbers are slightly different than the others. In order to have better resolution on the solution domain, other element numbers are evaluated. Accordingly, the relative error between 7.5K cell and 15K cell is 0.22%

and relative error between 15K and 30K cell is 0.002%. Therefore, it may be said that all grids have pretty close solutions at time step 20 s and the mesh independency is reached. Computational mesh structure is presented in Figure 2.19. Since model contains simple conduction and geometry is rectangular, hexahedral cell type is preferred. The cells can follow the geometry completely.

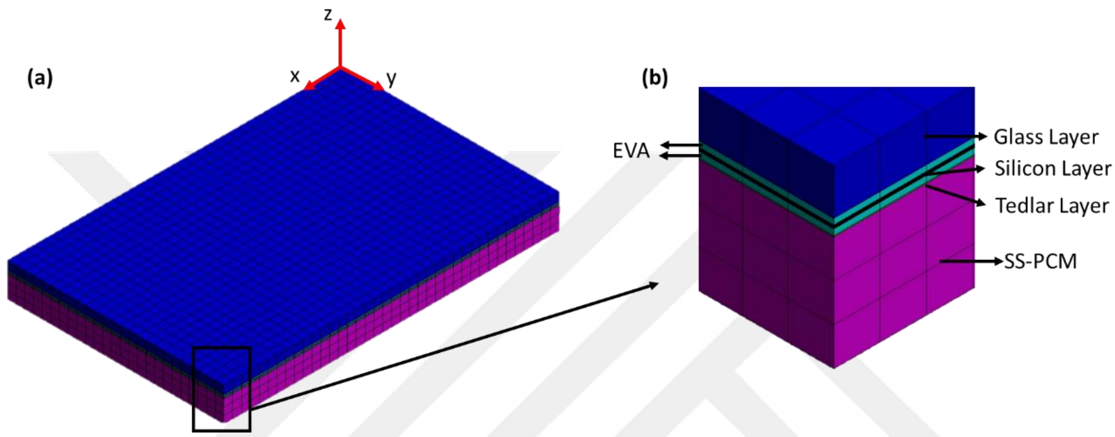

Figure 2.19 **(a)** Computational Domain Mesh Structure, **(b)** Detailed View

2.2.3.5 Time Step Independency Study

Time step independence studies are realized in order to understand and observe the effect of the selected time step value for analysis on the results. As mentioned before, the mesh which has 15K elements is chosen for the next studies. In time step independency study, that mesh is used for different time step sizes which are 5120s, 2560s, 1280s, 640s, 320s and 40s Efficiency of PV panel is presented in Figure 2.20.

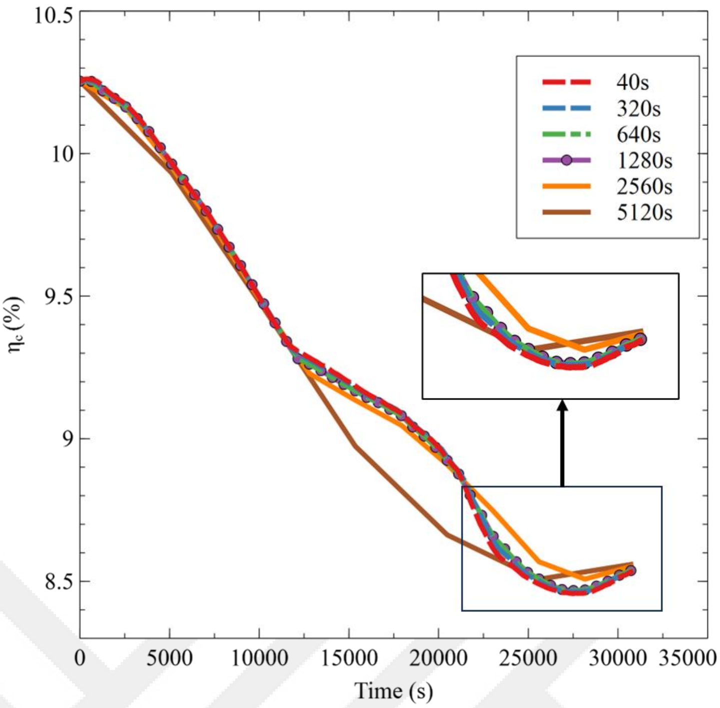

Figure 2.20 Cell Conversion Efficiency for Different Time Steps

All three results of 640s, 320s and 40s are following the close path as presented in Figure 2.20. 1280s, 2560s and 5120s results become a different than the others while approaching to the end. It may be said that the numerical model is time independent. However, 40s time step is selected for the next analyses due to suitability with time steps of collected data and resolution of results.

2.3 Uncertainty Analysis

Uncertainty analysis is important in order to avoid unexpected errors and provide accuracy to the measurement. The way in order to estimate the uncertainty in the experiments is calculated as in the following Eqn. 2.26 [60].

$$W_R = \sqrt{\left(\frac{\partial R}{\partial x_1} w_1\right)^2 + \left(\frac{\partial R}{\partial x_2} w_2\right)^2 + \cdots + \left(\frac{\partial R}{\partial x_n} w_n\right)^2} \qquad (2.26)$$

W_R is the overall uncertainty of the system with independent variables $(x_1, x_2 \ldots)$ and uncertainties of independent variables $(w_1, w_2 \ldots)$.Uncertainties of the used equipment are presented in Table 2.4.

Table 2.4 Uncertainties of the Test Equipment

Equipment	Uncertainty
Pyranometer	1%
T-type Thermocouple	+/- 1℃
Voltage	0.1%
Current	0.1%
Anemometer	3%

CHAPTER 3

RESULTS

3.1 Experimental Results

Experiments are conducted through two different configurations as explained in Chapter 2. In this part, the results of the PV panel test and thermal characterization experiment are evaluated.

3.1.1 PV Panel Test Results

The results of the PV panel tests are presented in this section of the thesis. Initially, a comparison of the provided PV panels was conducted based on their specifications. Although the panels are identical, their similarity was verified by measuring the open-circuit voltage of all three panels under the same conditions.

Temperature data, voltage values and current values are collected from the PV panels as already mentioned. The efficiencies of the PV panels are calculated by using the recorded data. According to the Marudaipillai et al. [28], cell conversion efficiency η_{ref} of the PV panel is calculated as on Eqn. 2.17. For panel 3, maximum electricity output is 6.43 W under 970 W/m^2. Panel 3 has 0.095 efficiency. Reference efficiency η_{ref} will be used in calculation of cell conversion efficiency η_c in numerical simulations.

The selected PV panel was mounted on the carcass structure. The test was conducted on the day 15.08.2024 and started at 06:54 and ended at 17:37. Irradiance and ambient temperature values are presented in Figure 3.1 and Figure 3.2. The temperature data taken from the center of the glass layer are exhibited in Figure 3.3 and the electricity generated by the PV panel is demonstrated in Figure 3.4.

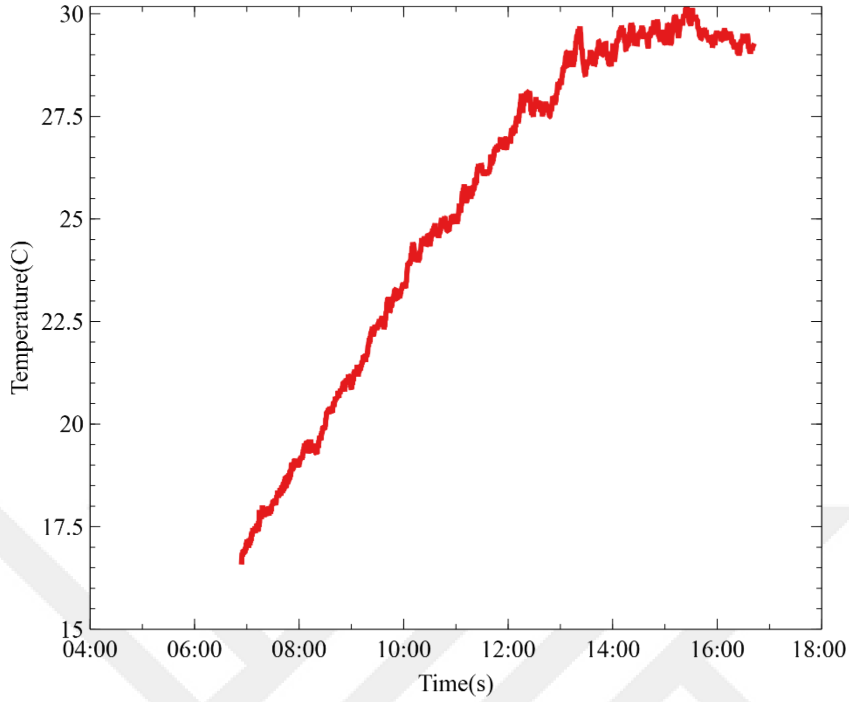

Figure 3.1 Ambient Temperature Variation – 15.08.2024

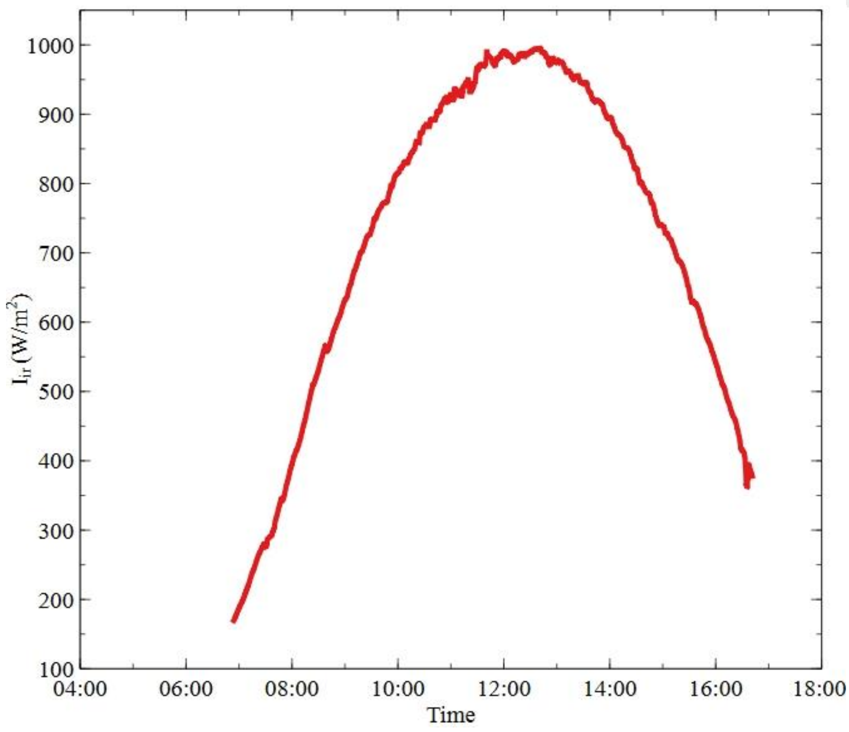

Figure 3.2 Irradiance Variation - 15.08.2024

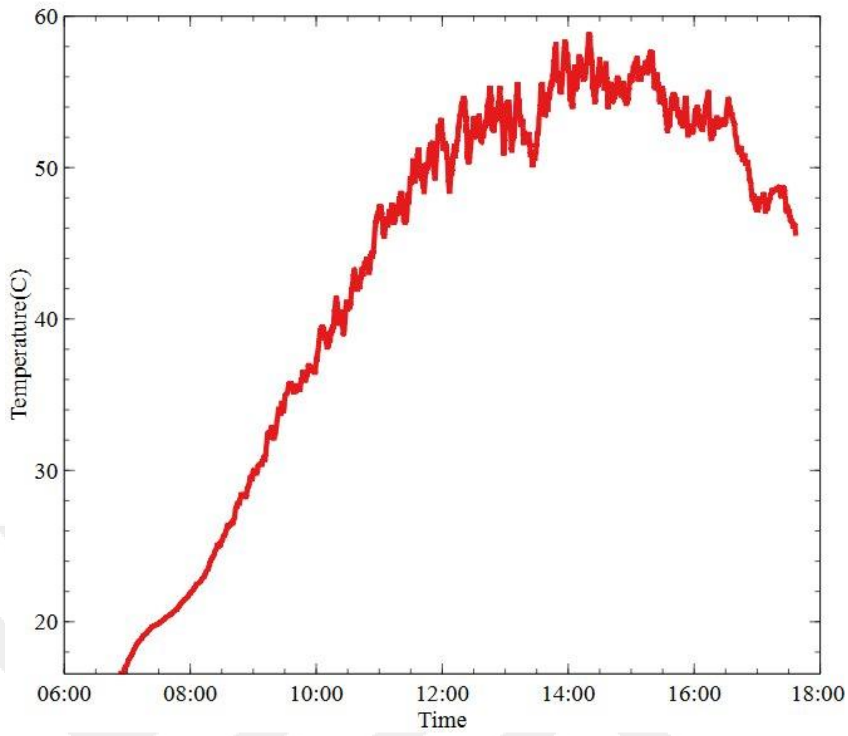

Figure 3.3 Temperature Variation of Glass Top Surface Center – 15.08.2024

The temperature of the glass top surface starts from below 20℃ in Figure 3.3. It increases with the rise of irradiance and ambient temperature. Approximately, after 09:40, the temperature rise slows down and reaches the maximum temperature at 14:19. The maximum temperature of glass top surface center is 58.94℃. This means that; the working temperature interval of the PV panel comprises the working temperature interval of the NPG's latent heat in a typical summer day.

The generated power during the test is presented in Figure 3.4. Generated power is low, but increases quickly in the morning. The PV panel achieves its maximum power generation at 12:40. Maximum power generated by the PV panel is 6.43 W, which is lower than the catalog values. At this moment, the irradiance is 970 W/m^2 and 27.6℃ , which are close to the standard conditions. The power generation showed that; the purchased photovoltaic panel is not working as expected.

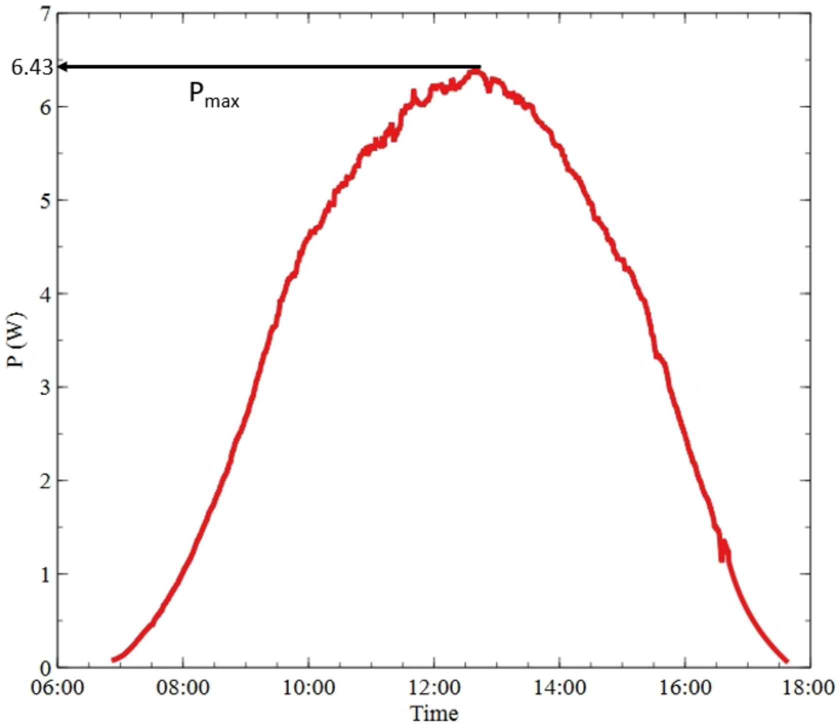

Figure 3.4 Generated Power by PV Panel – 15.08.2024

3.1.2 SS-PCM Thermal Characterization Experiment Results

An experimental setup is created to show the thermal characterization of the SS-PCM. The measured temperature inside PCM is used in this part. There is a very thin layer of SS-PCM in the aluminum casing. Thermocouples are located in the middle of the NPG. The aim of thin layer PCM is that, to provide PCM to behave like a bulk body and minimize the temperature gradient between the different locations of the PCM. The temperature change of PCM is shown in Figure 3.5 All locations inside SS-PCM have similar temperature values in Figure 3.5. Temperature uncertainty values are presented in Figure 3.5. The experiment is done twice in order to prove the repeatability of the conditions.

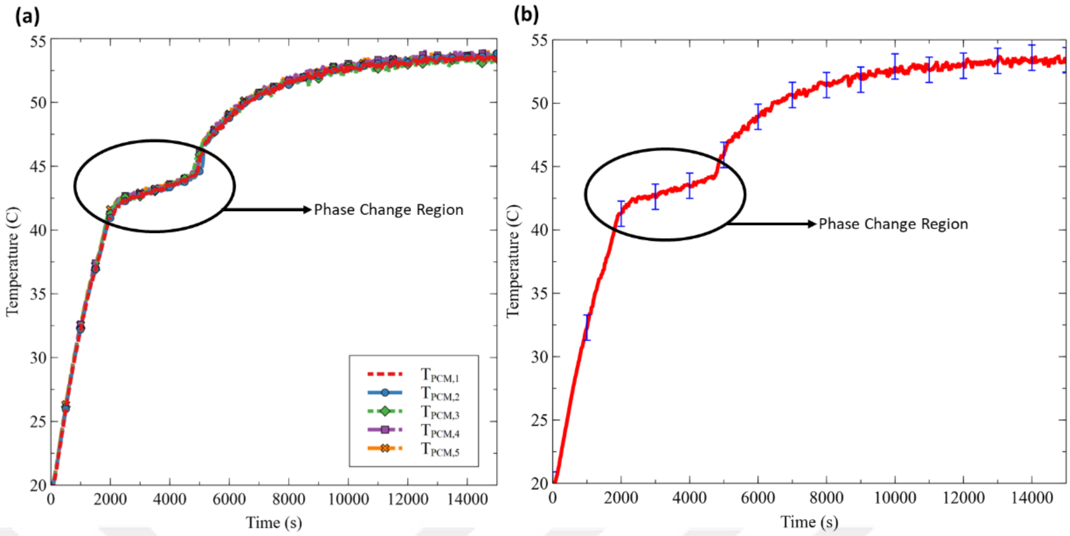

Figure 3.5 Temp. Variations of Thermocouples Inside PCM, **(a)** All Thermocouples, **(b)** Average Temp.

The temperature plot of the NPG is presented in Figure 3.5. As already explained in the previous chapters, NPG absorbs latent heat in a certain temperature range and this temperature interval can be observed in Figure 3.5. Latent heat absorption region is shown by dashed lines in Figure 3.5. T_∞ is equal to 20°C during the experiment period. Temperature values used in the energy balance calculations belong to the steady state. If one thermocouple is located on a surface, the temperature data is assumed as dominant on that face. The areas which the thermocouples are responsible for are presented in Figure 2.6 with blue dashed lines.

Convective heat transfer coefficient values are calculated with collected surface temperature data. On top surface of the aluminum casing, average temperature, $T_{Al,top1}$, is 54.47°C and, convective heat transfer coefficient, $h_{Al,top1}$, is 6.65±0.07 W/m^2K. For top surfaces of the base material, two temperature values are measured and for their symmetric areas, their temperatures are used. The top surface temperatures of base material,$T_{b,top1}$ and $T_{b,top2}$, equal to 29.7°C and 32.7°C respectively. Convective heat transfer coefficients belonging to them, $h_{b,top1}$ and $h_{b,top2}$, are calculated as 6.35±0.14 W/m^2K 6.60±0.17 W/m^2K respectively. For side surfaces of the base material, two temperature values are measured and for their symmetric areas, their temperatures are used. The measured temperature values for side surfaces of base material, $T_{b,side1}$ and $T_{b,side2}$ are equal to 24.50℃ and 24.63℃ in order. Convective heat transfer coefficients calculated with those temperatures, $h_{b,side1}$ and $h_{b,side2}$, are equal to 1±0.14 W/m^2K for both surfaces. For bottom surfaces of the base material, three temperature values are measured and for the symmetric areas of two, their temperatures are used. The other one is at the center of the bottom. The temperature at the center, $T_{b,bottom3}$, is equal to 32.95℃ and the other temperatures,$T_{b,bottom1}$ and $T_{b,bottom2}$ are measured as 22.30℃ and 22.80℃. Convective heat transfer coefficients belonging to bottom surface of base material, $h_{b,bottom1}$, $h_{b,bottom2}$ and $h_{b,bottom3}$ are calculated as 3.01±0.266 W/m^2K, 3.09±0.22 W/m^2K and 3.23±0.06 W/m^2K, respectively. Discretized heat transfer is illustrated in Figure 3.6. Steady-state heat transfer rates are presented in Table 3.1.

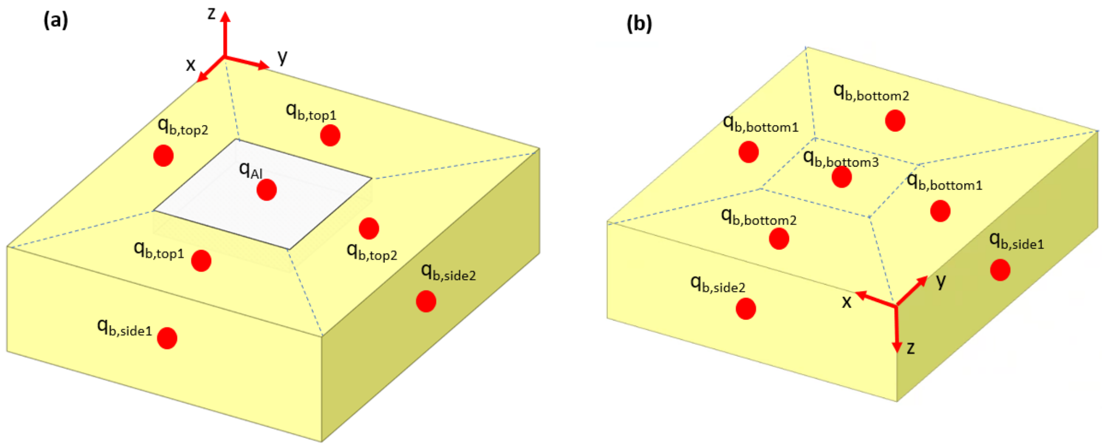

Figure 3.6 Discretized Heat Transfer **(a)** Isometric Top-Down View, **(b)** Isometric Bottom-Up View

Table 3.1 Steady-State Heat Transfer Rates

Heat Transfer Rates	**Value (W)**
q_{Al}	1.2±0.04
$q_{b,top1}$	0.47±0.07
$q_{b,top2}$	1.23±0.15
$q_{b,side1}$	0.07±0.04
$q_{b,side2}$	0.08±0.05
$q_{b,bottom1}$	0.14±0.02
$q_{b,bottom2}$	0.05±0.02
$q_{b,bottom3}$	0.19±0.042
$\mathbf{q_{total}}$	3.43±0.19

Total heat transfer is calculated as 3.43±0.19 W by using the values in Table 3.1. Calculated released heat value is close to the given input value which is 3.5 W. Relative difference between calculated heat transfer rate and power input is 2 %. The total power passing through aluminum casing is calculated as 1.2 W at steady state, with $h_{Al,top}$ and radiative heat transfer from aluminum. This power value is used in thermal circuit approach inside of aluminum casing. In that evaluation, the thermal conductivity of NPG is calculated as 0.27±0.001 $W/m.K$. Calculated value is in the interval of 0.15-0.42 W/mK [37]. Plot of the thermal characterization experiment results is presented in Figure 3.7.

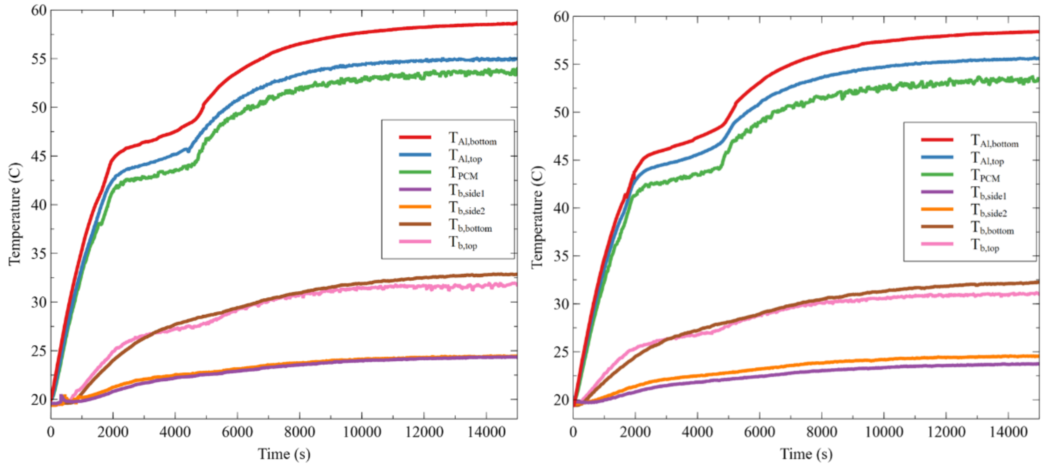

Figure 3.7 PCM Thermal Characterization Exp., **(a)** First Trial, **(b)** Second Trial

The thermal characterization of PCM is done twice as mentioned before in order to prove the repeatability of the experiment. As presented in Figure 3.7, the temperature values are almost similar. The temperature difference between $T_{Al,top}$ at the end of experiment is 0.59℃. Therefore, it is obvious that established experiment is repeatable and a guide for the numerical analysis.

The target of this experimental study is the characterization of neopentyl glycol. The experiment showed that neopentyl glycol has latent heat absorption characteristics as mentioned in the literature. Moreover, the thermal conductivity of the PCM is obtained. These obtained and proven data will guide numerical analysis.

3.2 Numerical Analysis Results

Numerical analyses are done to investigate the thermal management of PV panel with SS-PCM. Ideal SS-PCM configuration which gives the best solution for thermal management of PV panel is determined. Until modelling the SS-PCM integrated PV panel, PV panel modelling and SS-PCM modelling are completed to be sure about the accurate modelling of them since the main numerical analyses contains both of them.

Numerical analysis results is divided into three parts. Two of them are validation of PV Panel Test and Characterization of SS-PCM. The validity of those simulations is a guide to SS-PCM integrated PV Panel analyses.

Numerical validations are introduced, in this section. SS-PCM integrated PV panel configurations and without-PCM cases' numerical studies are evaluated and compared.

3.2.1 Numerical Model Validation for PV Panel Test Results

To ensure the accuracy of the created PV panel's numerical model, the analysis result is validated with PV panel test results. On the day of 15.08.2024, the experiment was realized with the panel which is most compatible with the catalog. The irradiance, ambient temperature, and temperature data of PV panels were collected. The comparison plot of the temperature of the glass top center is presented in Figure 3.8.

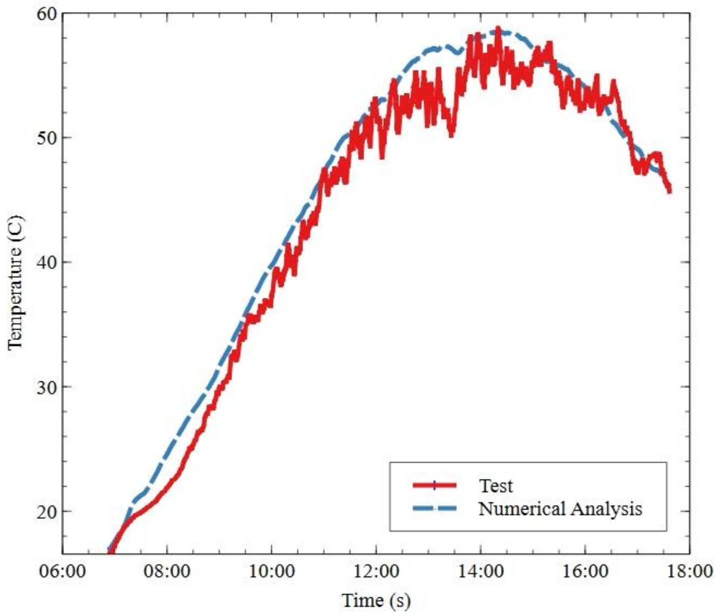

Figure 3.8 Temperature Variation of PV Panel Glass Top Surface Center

The test started at 06:54 and ended at 17:37, which means the test was run for 38560 seconds. Analysis results and test results have similar trends and close values in Figure 3.8. The maximum temperature value of the test is equal to 58.9℃. The maximum temperature value of the analysis is equal to 58.5℃. The maximum temperature values and the moments those temperatures occur are close to each other. Therefore, it may be said that validation of the numerical model is done with these validation results and the numerical model for PV Panel could be used for the next numerical analysis and evaluations of different PV panel model configurations.

3.2.2 Numerical Model Validation for SS-PCM Thermal Characterization Results

The experiment which is done to show the thermal characterization of the NPG is modeled numerically. A heat flux is applied from bottom of the computational domain which is aluminum casing. Acquired data from the experiment is applied as input heat flux in time domain. Sum of released heat from top surface of aluminum and stored sensible heat by NPG until phase transition and after phase transition is used. Sum of released heat from top surface of aluminum and absorbed latent heat by PCM is applied during the phase change. Heat flux calculations are done for certain time steps. To compare the results of the numerical analysis and the test, SS-PCM temperatures are used. The temperature plot of the test and analysis is shown in Figure 3.9.

Numerical analyses are validated with experimental results as in Figure 3.9. The R-square value is calculated as 0.94. The calculated R-square value shows that numerical model of the phase change material is close to the test case and it may be applied to the numerical analysis of the PV panel and SS-PCM configuration.

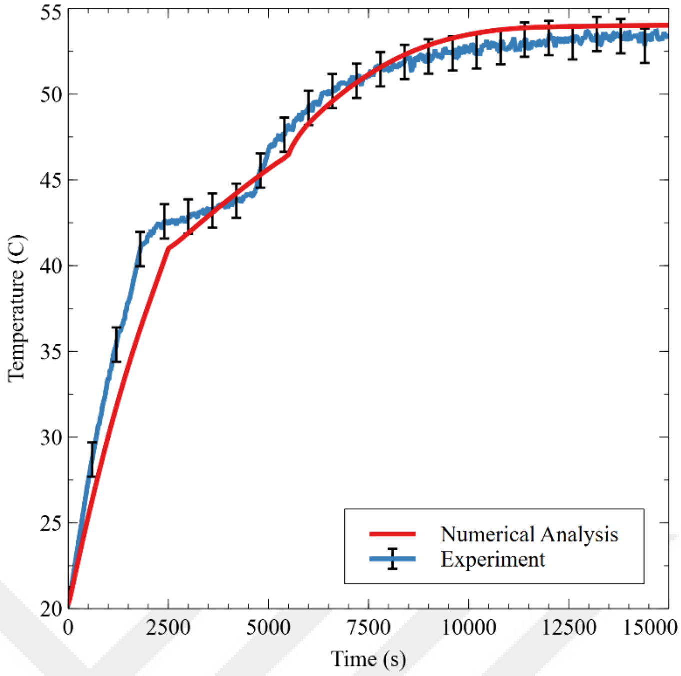

Figure 3.9 SS-PCM Temperature Variation

3.2.3 SS-PCM Integrated PV Panel Results

The numerical validations of the PV panel model and SS-PCM model were performed based on experimental data. In this section of the thesis, the impact of integrating SS-PCM to the PV panel and its performance is analyzed. Comparisons are made between the PV panel without PCM and panels with varying SS-PCM thicknesses.

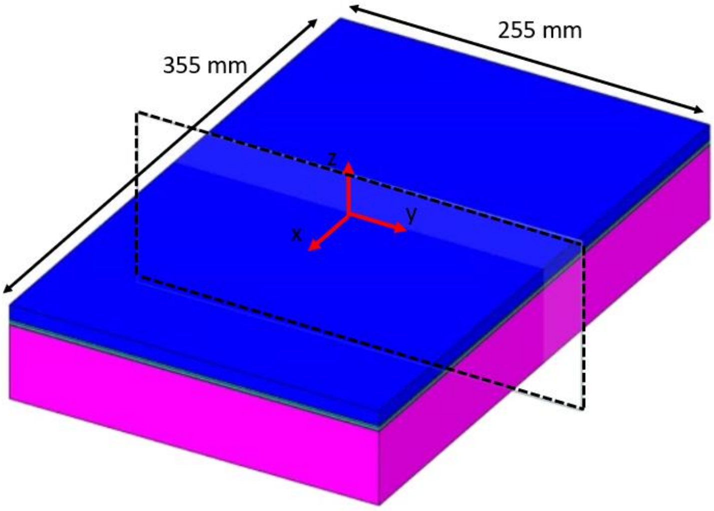

Figure 3.10 Contour Plane

The depicted plane in Figure 3.10 is used for obtaining temperature contour and phase change fraction contour. $x = 0$ is the contour plane. The geometry in Figure 3.10 belongs to the complete geometry. During the simulations for the phase change material and PV panel configuration, boundary conditions are irradiance, ambient temperature and wind velocity measured on 15.08.2024. Simulations start from 06:54 and finish at 17:41. Simulation duration is 38560 s. The collected data was used as input and given as profile into the Ansys FLUENT except wind velocity. Wind velocity is measured three times in the day and indicated as $1.4\,m/s$. Irradiance and ambient temperature input are represented in Figure 3.1 and Figure 3.2.

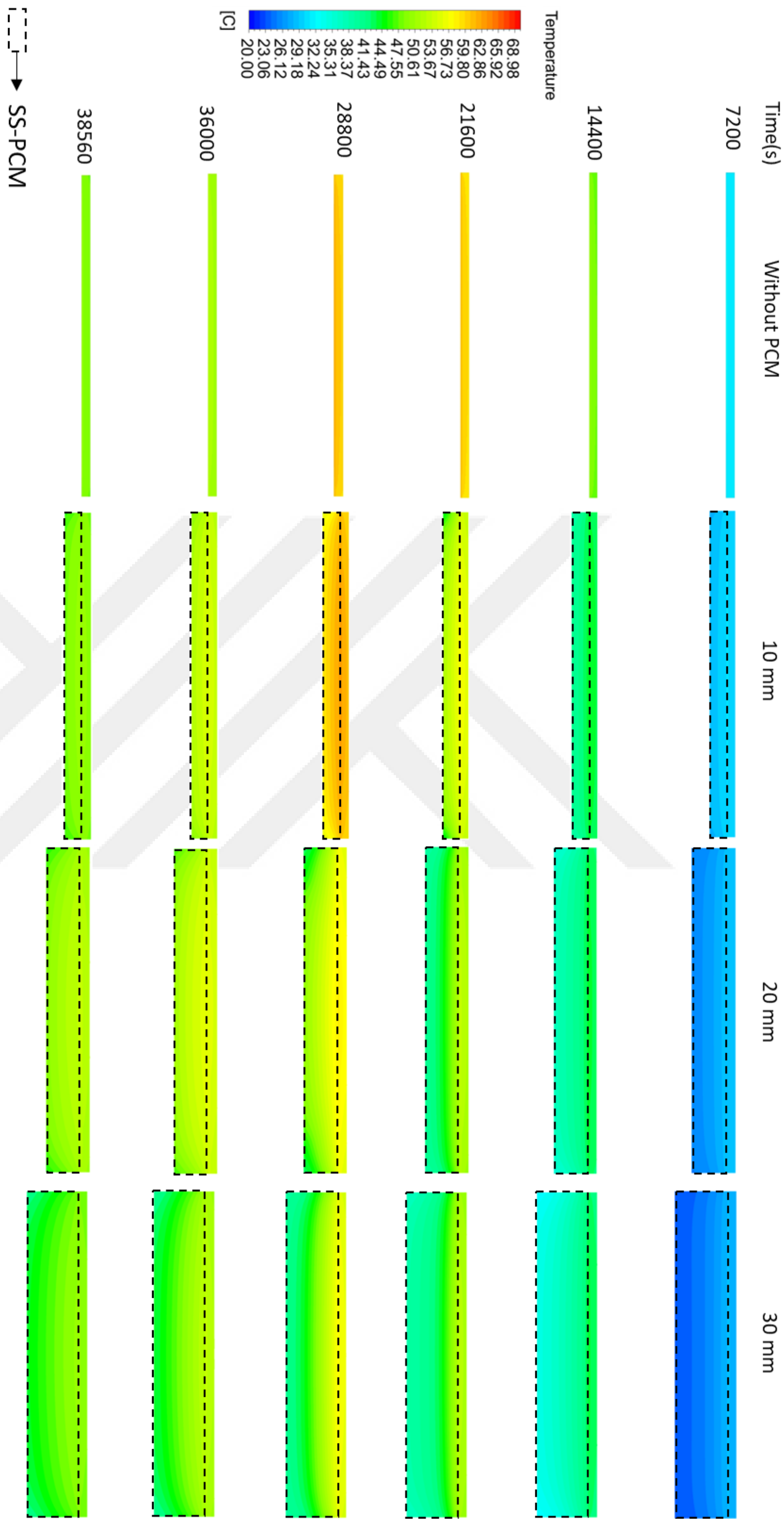

Figure 3.11 Temperature Variation of SS-PCM Integrated PV Panels

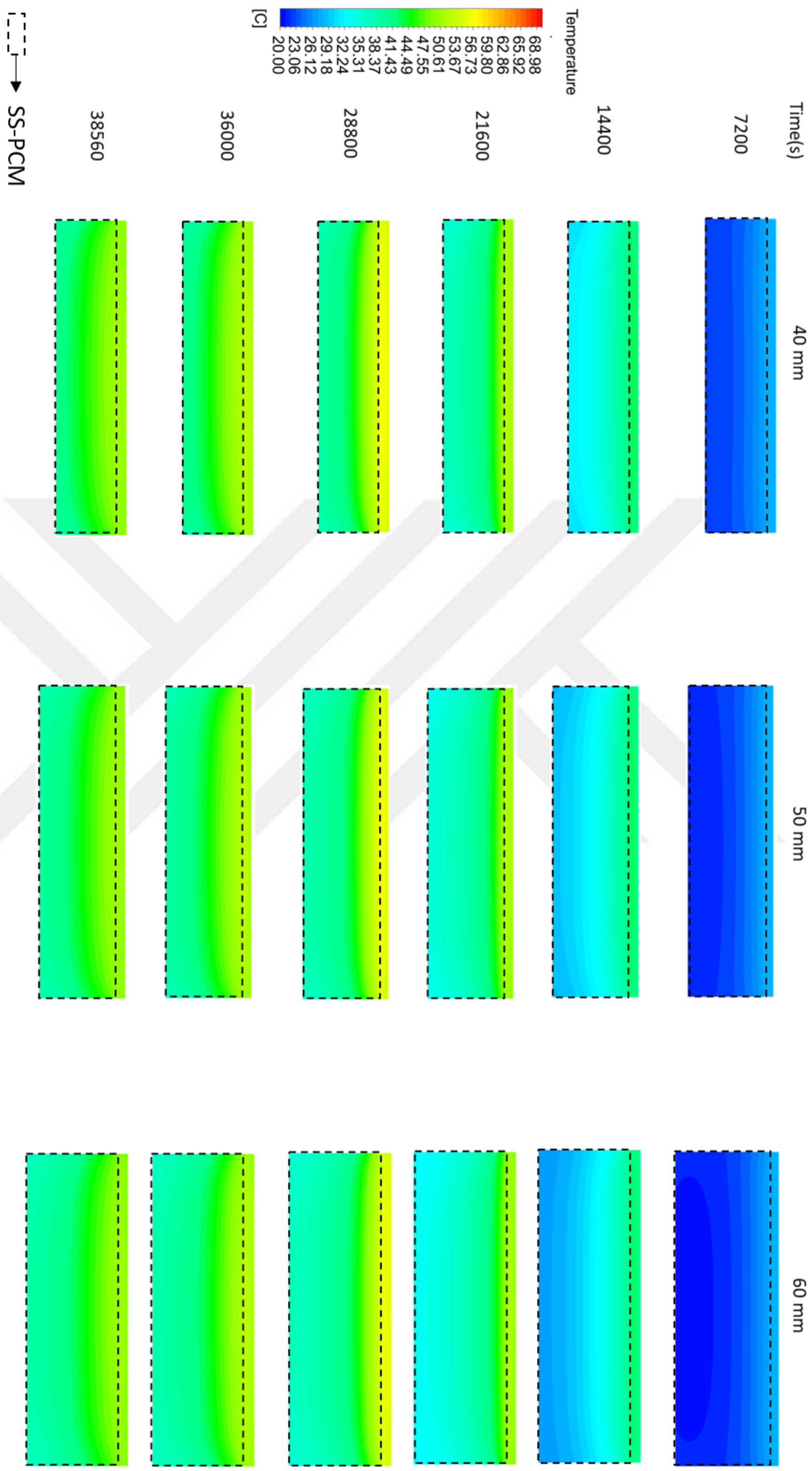

Figure 3.11 Temperature Variation of SS-PCM Integrated PV Panels (continued)

The temperature contours of the numerical analysis with respect to time are demonstrated in Figure 3.11. The SS-PCM region is indicated as a wireframe. Temperature contours are taken from the middle of the PV panel model as in Figure 3.10. As previously mentioned, the silicon layer of the PV panel acts as a heat source, while the top glass layer is subjected to convection and irradiance boundary conditions. The walls and the bottom of the numerical domain are governed by natural convection boundary conditions. As shown in the temperature contour figures, the upper part of the photovoltaic panel is warmer than the other sections. Since the side regions of the panel are influenced by natural convection boundary conditions, the areas near the side walls exhibit lower temperatures. Temperature gradients can be observed in the figures. For all cases, it may be said that the maximum temperatures are seen around the 28800^{th} second.

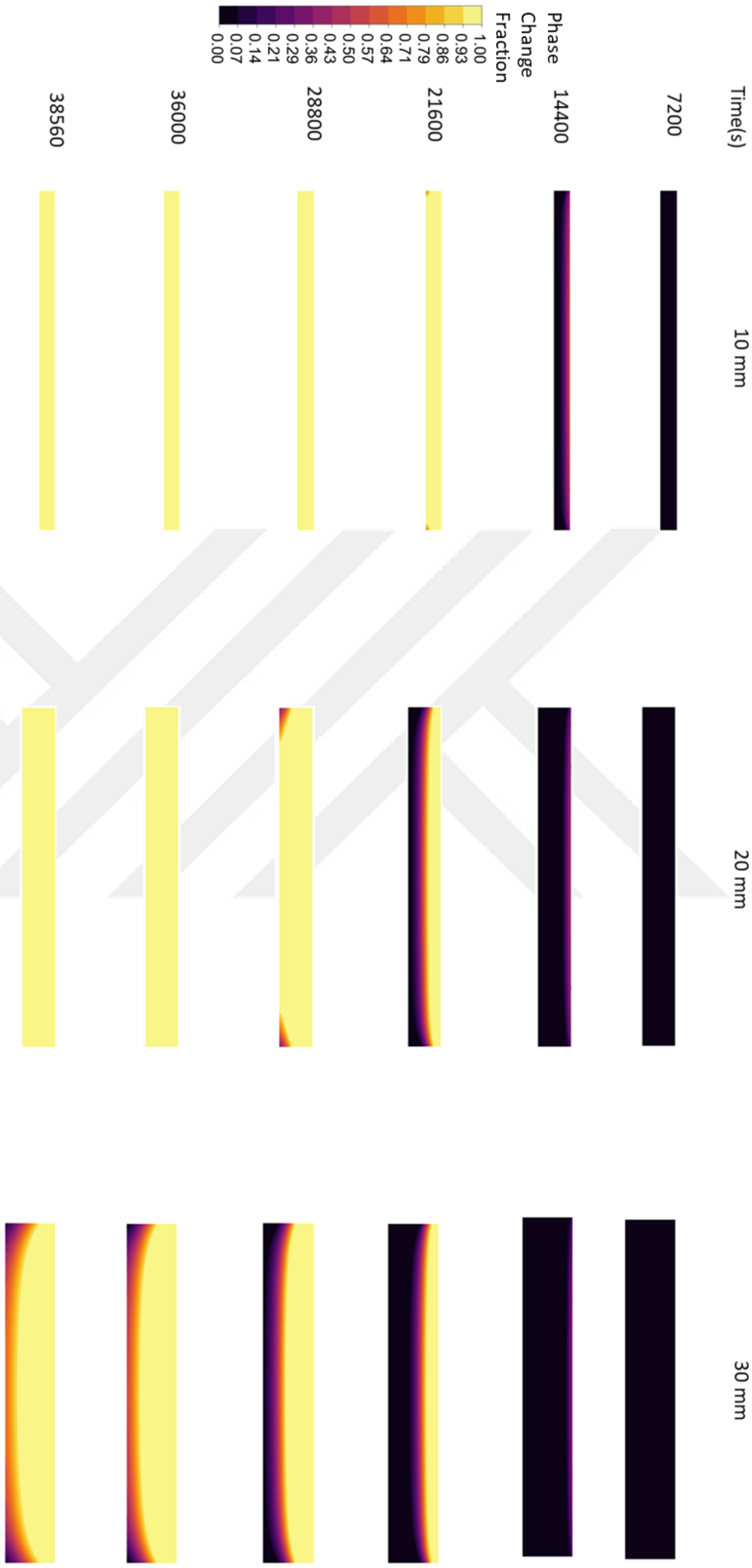

Figure 3.12 Phase Change Variation of SS-PCM Integrated PV Panel

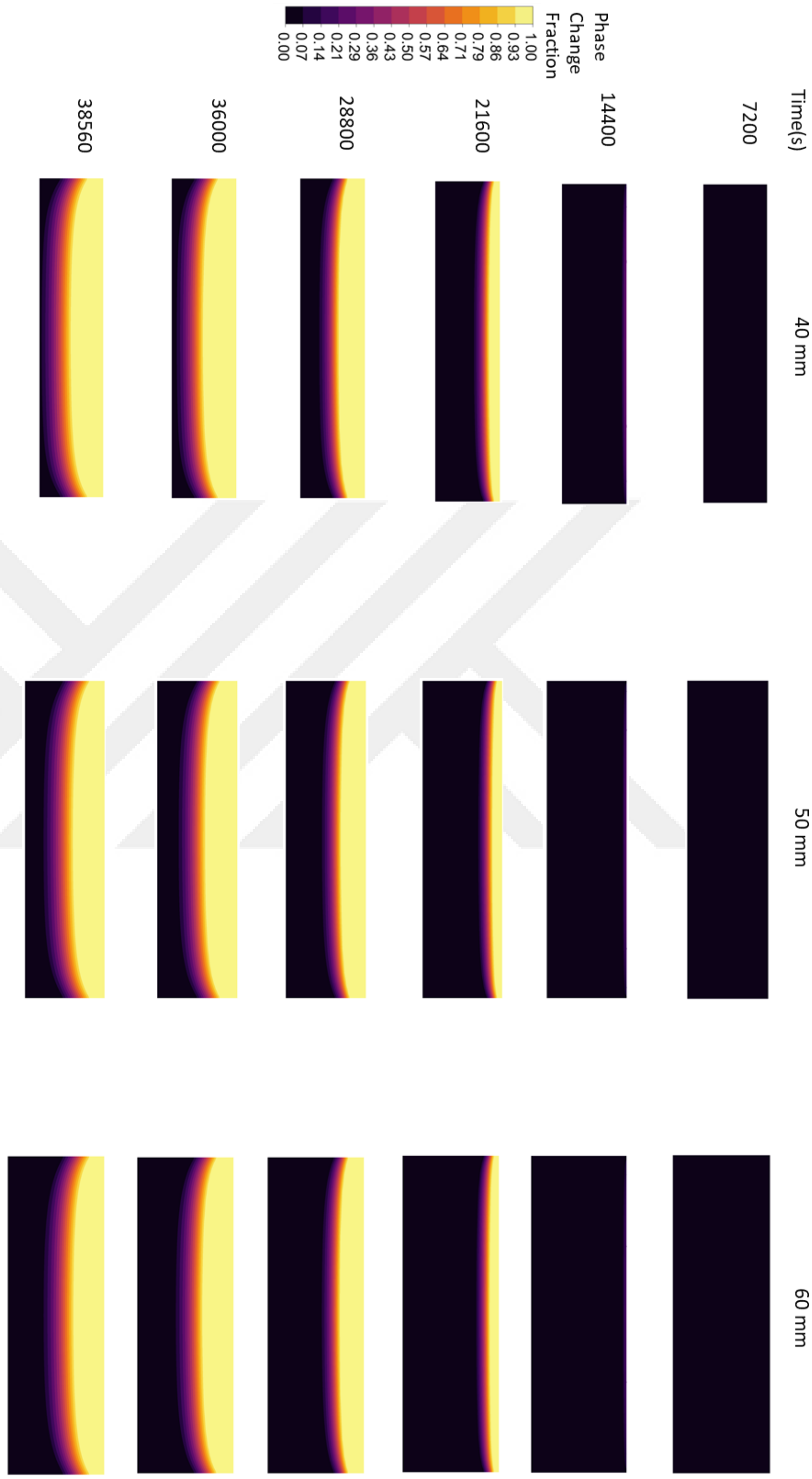

Figure 3.12 Phase Change Variation of SS-PCM Integrated PV Panel (continued)

Phase change fractions of the PCM cases are demonstrated in Figure 3.12. For the 10 mm and 20 mm PCM thickness cases, the phase change material undergoes a complete phase transition. By the end of the analysis, although the system's temperature decreases, the material remains in the gamma phase. In contrast, for the 30 mm and 40 mm PCM thickness cases, the phase change is less pronounced compared to the 10 mm and 20 mm cases. For thicknesses beyond 40 mm, most of the phase change material remains in its initial phase. These results suggest that 10 mm and 20 mm PCM thicknesses are insufficient to maintain performance throughout the day, while the 50 mm and 60 mm cases exceed the PV panel's requirements, as the material does not fully complete its phase change within the designated time.

Numerical analysis is done for different thicknesses of NPG and without-PCM case. The given dimensions in the legend of Figure 3.13 and Figure 3.14 are the thicknesses of the PCM during the simulations. The top surface glass temperature of the photovoltaic panel and its efficiency are plotted based on the numerical analysis results in Figure 3.13 and Figure 3.14.

As a result, in the without-PCM case, the temperature at the center of the top glass surface increases continuously with irradiance and ambient temperature but eventually begins to decrease due to environmental conditions. Similar behavior may be seen in also on Figure 3.14, as already said, if the temperature of the photovoltaic panel increases, its efficiency decreases. The efficiency of the PV panel for without-PCM case shows the quite opposite behavior to the temperature of it. The average temperature of the without-PCM case is equal to 47.49℃ and the average η_c of the without-PCM case panel is equal to 9.05% in the day.

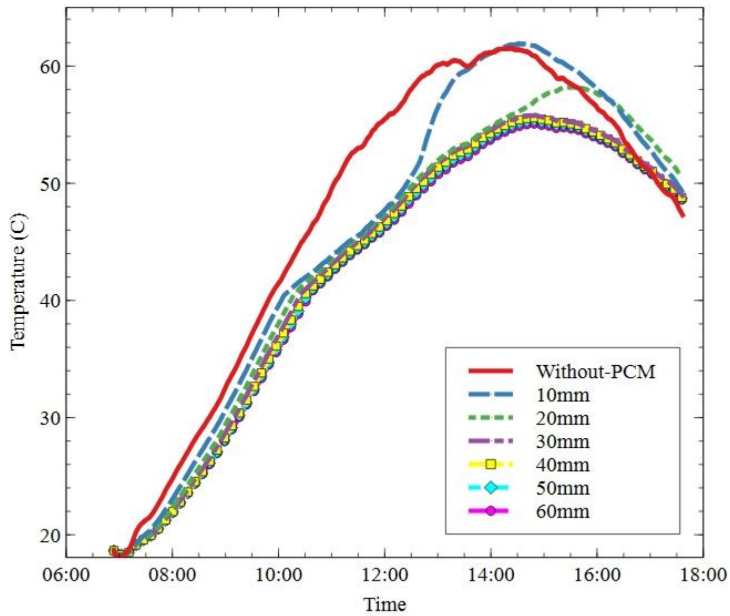

Figure 3.13 Temperature Variation of Glass Top Surface Center

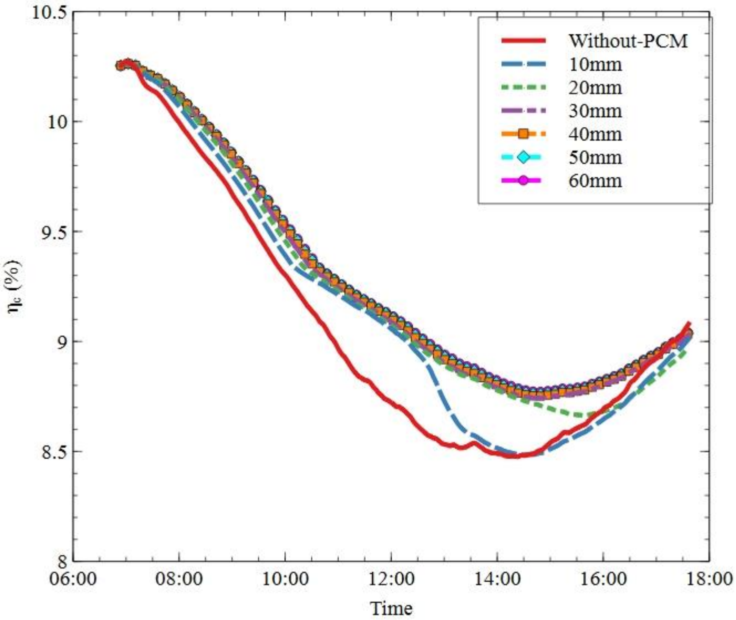

Figure 3.14 Cell Conversion Efficiency of SS-PCM Integrated PV Panel

All of the configurations have a drop of increasing speed of the temperatures for the cases with SS-PCM in Figure 3.13. It starts close to 41 ℃ which is the phase change starting temperature of the neopentyl glycol. The SS-PCM reaches full phase change for 10 mm and 20 mm cases. On the other hand, for 30 mm case, PCM reaches 0.85 change; for 40 mm case, PCM reaches 0.64 change; for 50 mm case 0.49 change and for 60 mm case 0.40 change throughout the day.

The temperatures are below the temperatures of the without-PCM case for all of the SS-PCM cases. The efficiencies are above of the without-PCM case. Average temperatures and average efficiencies of the panels are calculated from analysis results. On top surface of the glass, without-PCM case has 47.49℃ average temperature. PCM cases have average temperatures 45.77℃, 44.14℃, 43.14℃, 42.87℃, 42.84℃, 42.82℃ from 10 mm to 60 mm respectively. For every step, average temperature is decreasing. If the thickness is getting higher, average temperatures are approaching each other, converging. After 40 mm thickness NPG, the average temperatures are much closer to ignore thicker ones. The relative temperature difference ratio between 40 mm and 50 mm thickness configuration is 0.075% which is a low value and does not show any considerable change after that step. Therefore, 40 mm thickness configuration may be the suitable choice for the design and this thick NPG causes 9.74% decrease for average temperatures of glass top surface.

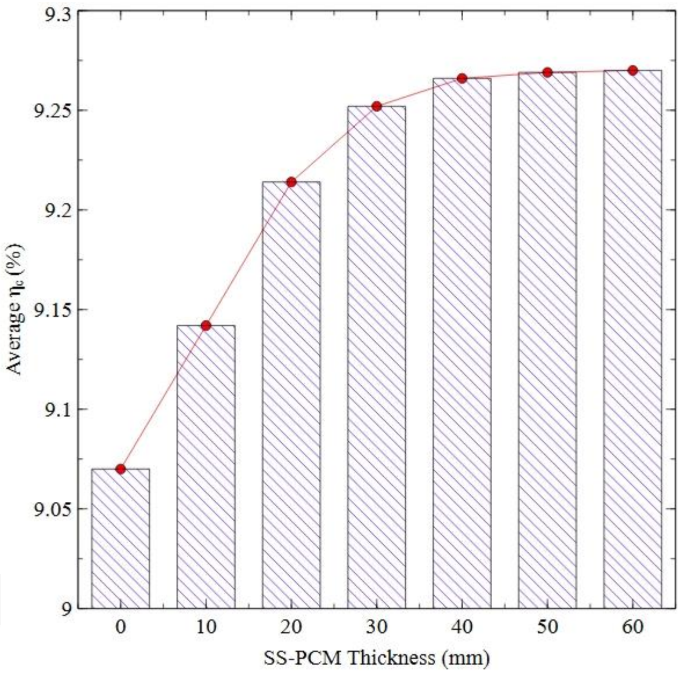

Figure 3.15 Average Cell Conversion Efficiency of Different SS-PCM Thicknesses

The average efficiency values are presented in Figure 3.15. After 40 mm thickness configurations, the efficiency of the panel does not show much change in the efficiency of it. As much as PCM thickness gets higher, the cost of the configuration increases. Increase in thickness does not make a significant contribution after a certain thickness value. Therefore, it may be said that 40 mm neopentyl glycol use with photovoltaic panels can be beneficial, enough and efficient in order to increase the efficiency and performance of the photovoltaic panel. 40 mm NPG leads to cell conversion efficiency increase from 9.05% to 9.27%.

CHAPTER 4

CONCLUSION

Cell conversion efficiency improvement of PV panel is investigated with SS-PCM in this thesis. Increasing the energy conversion efficiency of a PV panel means more electricity produced by a renewable energy generation way.

SS-PCM is used to apply thermal management to the PV panel and neopentyl glycol is selected as SS-PCM. These materials have a feature that absorbs energy in a certain temperature range although the phase of the material remains solid, since it changes its crystal structure during this time interval. As the material remains solid, there is no need for special encapsulations and there will not be a leakage problem. By using SS-PCM, the PV panel energy conversion performance is evaluated.

The investigation started with implementing tests in summer at Middle East Technical University. Three photovoltaic panels were purchased in order to see the compatibility of the photovoltaic panel performance with catalog data. Under the same daylight, open-circuit voltages of the three PV panels are compared and one of the PV panels has been selected as the sample. PV panel is tested under daylight to evaluate its performance and to create inputs for the PV panel numerical modelling. The obtained ambient temperature, irradiance, wind velocity, surface temperature of the PV panel and generated power during the tests are utilized as boundary conditions in the numerical solutions. Results of the test are used for validation of created numerical model for PV panel.

Another experimental study is conducted in order to investigate the thermal characterization of the NPG in laboratory conditions. PCM in an aluminum casing is exposed to constant heat flux. The temperature data collected during the experiment have proven that NPG has latent heat absorption in a certain temperature interval while remaining solid. Moreover, the thermal conductivity of the NPG is calculated as 0.27 $W/m.K$, which is close to literature information, to contribute to numerical analysis. The experiment is done to observe NPG's phase transition and to calculate its thermal conductivity since there are different thermal conductivity values in the literature. Furthermore, collected temperature data are used to validate the created numerical model for NPG, since numerical modelling of the SS-PCM is critical in this thesis.

SS-PCM integrated PV panel modelling includes both PV panel and SS-PCM. Therefore, PV panel and thermal characterization experiment are modelled numerically. Numerical analyses are started with grid independence and time step independence analysis. In order to make results of the created models for PV panel and thermal characterization experiment not changing with different element numbers and time steps and reduce solution time of the analysis, those applications are done. The created models for PV panel and thermal characterization experiment are validated with experimental results after independency studies. Numerical models yielded consistent results with experimental outputs. It was found that created models are suitable for modeling PV panel and SS-PCM together. Grid independency and time independency study are done for SS-PCM integrated PV panel. Final analyses are done after proving the created model is grid independent and time independent. The NPG integrated PV panel configuration numerical models are run in order to analyze and evaluate the performance of the PV panel with SS-PCMs. The results represent that the phase change of the NPG slows down the temperature increase of the PV panel and increases the efficiency of the PV panel. As much as the thickness of the NPG increases, the efficiency rise slows down. The outcome of the numerical results shows that the PV panel and SS-PCM combination may be useful and beneficial. Since certain case is just researched recently, the outcomes of the study are significant. Studied all thickness values contribute to the efficiency of PV panel. In conclusion, 40 mm NPG integration may be useful and enough to get the ideal performance of the PV panels. When the phase change contours of the materials are checked, during the numerical case solution for a certain time range, the 40 mm PCM thickness case changes its phase mostly. The other cases either changed their phase already and fell short, or could not change their phase in that time range. The current configuration decreased the average temperature of top surface of the glass layer 9.74%. The average cell conversion efficiency increased from 9.05% to 9.27%. The current results showed that SS-PCM integration to the PV panel may be helpful to increase the power generation of PV panels. Especially, large-scale PV panels are taking on the task of supplying electricity to cities. Considering the benefits provided by SS-PCM in large-scale panels, the increases mentioned in the thesis will significantly enhance power generation in PV panels.

The following studies may be realized in order to investigate the performance of photovoltaic panels and solid-solid phase change material configuration in the future:

- A well-fabricated phase change material integrated photovoltaic panel which has small contact resistance between the tedlar layer and solid-solid PCM to realize the experiments of real configuration should be manufactured.
- Different solid-solid phase change materials may be investigated with photovoltaic cells.
- Integration of metal fins, metal foams or metal nanoparticles into the solid-solid phase change materials may be examined to improve the performance of photovoltaic panels.
- SS-PCM integration to the large-scale PV panels may be modelled and investigated experimentally.
- Application of solid-solid phase change material to the photovoltaic panels may be researched with active cooling methods.
- Economic analysis may be done for use of solid-solid phase change material with photovoltaic panels.

REFERENCES

[1] Mohammadpour, J., Salehi, F., Sheikholeslami, M., & Lee, A. (2022). A computational study on nanofluid impingement jets in thermal management of photovoltaic panel. *Renewable Energy*, *189*, 970-982.

[2] Özcan, Z., Gülgün, M., Şen, E., Çam, N. Y., & Bilir, L. (2021). Cooling channel effect on photovoltaic panel energy generation. *Solar Energy*, *230*, 943-953.

[3] Hussien, A., Eltayesh, A., & El-Batsh, H. M. (2023). Experimental and numerical investigation for PV cooling by forced convection. Alexandria Engineering Journal, 64, 427-440.

[4] Ahmad, A., Navarro, H., Ghosh, S., Ding, Y., & Roy, J. N. (2021). Evaluation of new pcm/pv configurations for electrical energy efficiency improvement through thermal management of pv systems. *Energies*, *14*(14), 4130.

[5] Kumar, K. S., Revanth, S., Sanjeev, D., Kumar, P. S., & Surya, P. (2021). Experimental investigation of improving the energy conversion efficiency of PV cell by integrating with PCM. *Materials Today: Proceedings*, *37*, 712-716.

[6] Sharifpur, M., Ahmadi, M. H., Rungamornrat, J., & Mohsen, F. M. (2022). Thermal management of solar photovoltaic cell by using single walled carbon nanotube (SWCNT)/water: Numerical simulation and sensitivity analysis. Sustainability 14, 11523.

[7] Ma, T., Li, Z., & Zhao, J. (2019). Photovoltaic panel integrated with phase change materials (PV-PCM): technology overview and materials selection. *Renewable and Sustainable Energy Reviews*, *116*, 109406.

[8] Wang, C., Li, Q., Wang, L., & Lan, X. (2016). Phase transition of neopentyl glycol in nanopores for thermal energy storage. *Thermochimica acta*, *632*, 10-17.

[9] Kuta, M., & Wójcik, T. M. (2015). Phase change materials in energy sector-applications and material requirements. In EPJ Web of Conferences (Vol. 92, p. 02043). EDP Sciences.

[10] Pillai, P. B., Venkitaraj, K. P., Suresh, S., Ali, H. M., Aswin, G., Abhishek, R., ... & Kumar, A. (2025). Application of a Solid–Solid Nanocomposite PCM for Thermal Management of a Solar PV Panel. In *Phase Change Materials for Thermal Energy Management and Storage* (pp. 275-303). CRC Press.

[11] Ali, M., Iqbal, M. H., Sheikh, N. A., Ali, H. M., Shehryar Manzoor, M., Khan, M. M., & Tamrin, K. F. (2017). Performance investigation of air velocity effects on PV modules under controlled conditions. *International Journal of Photoenergy*, *2017*(1), 3829671.

[12] Özcan, Z., Gülgün, M., Şen, E., Çam, N. Y., & Bilir, L. (2021). Cooling channel effect on photovoltaic panel energy generation. *Solar Energy*, *230*, 943-953.

[13] Javidan, M., & Moghadam, A. J. (2021). Experimental investigation on thermal management of a photovoltaic module using water-jet impingement cooling. *Energy Conversion and Management*, *228*, 113686.

[14] Mohammadpour, J., Salehi, F., Sheikholeslami, M., & Lee, A. (2022). A computational study on nanofluid impingement jets in thermal management of photovoltaic panel. *Renewable Energy*, *189*, 970-982.

[15] Shiravi, A. H., & Firoozzadeh, M. (2020). Thermodynamic and Environmental Assessment of Mounting Fin at the Back Surface of Photovoltaic Panels. *Journal of Applied and Computational Mechanics*.

[16] Elsafi, A., & Gandhidasan, P. (2015). Performance of a photovoltaic or thermal double-pass solar air heater with different fin configurations. *J. Clean Energy Technol*, *3*, 28-33.

[17] Del Rio, J. A. S., Ardila, Y. R., Sánchez, A. R., Quintana, E. C., Sanin-Villa, D., González, C. A., & Luna-Del Risco, M. (2023). Numerical

Study of the Efficiency of a Solar Panel with Heat Sinks. *CFD Letters*, *15*(4), 43-52.

[18] Wu, G., Liu, Q., Wang, J., & Sun, B. (2021). Thermal analysis of water-cooled photovoltaic cell by applying computational fluid dynamics. *Journal of Thermal Analysis and Calorimetry*, *144*, 1741-1747.

[19] Rosli, M. A. M., Latif, I. A. F., Nawam, M. Z., Saadun, M. N. A., Jarimi, H., Sharif, M. K. A., & Ali, S. (2021). A simulation study on temperature uniformity of photovoltaic thermal using computational fluid dynamics. *Journal of Advanced Research in Fluid Mechanics and Thermal Sciences*, *82*(1), 21-38.

[20] Babavali, S. F., Devi, N. L., Kaliappan, S., Garg, N., Nagalakshmi, V., & Rajagopalan, N. R. (2023). Thermal management of PV panel through the circulation of a nano-MgO/water-based nanofluid. *Materials Today: Proceedings*.

[21] Sharifpur, M., Ahmadi, M. H., Rungamornrat, J., & Mohsen, F. M. (2022). Thermal management of solar photovoltaic cell by using single walled carbon nanotube (SWCNT)/water: Numerical simulation and sensitivity analysis. Sustainability 14, 11523.

[22] Savvakis, N., & Tsoutsos, T. (2016). Phase Change Materials in Photovoltaic’s: The Assessment of System Performance in the Present Mediterranean Climate Conditions. *Power Systems, Energy Markets and Renewable Energy Sources in South-Eastern Europe*.

[23] Aneli, S., Arena, R., & Gagliano, A. (2021). Numerical Simulations of a PV Module with Phase Change Material (PV-PCM) under Variable Weather Conditions. *International Journal of Heat & Technology*, *39*(2).

[24] Ma, T., Zhao, J., & Han, J. (2017). A parametric study about the potential to integrate phase change material into photovoltaic panel. *Energy Procedia*, *142,* 648-654.

[25] Bria, A., Raillani, B., Chaatouf, D., Salhi, M., Amraqui, S., & Mezrhab, A. (2023). Effect of PCM thickness on the performance of the finned PV/PCM system. *Materials Today: Proceedings*, *72*, 3617-3625.

[26] Abd El-Hamid, M., & Wei, G. (2024). Effect of varying the thermophysical properties of phase change material on the performance of photovoltaic/thermal-PCM hybrid module numerically. *Journal of Energy Storage*, *86*, 111326.

[27] Rajvikram, M., Leoponraj, S., Ramkumar, S., Akshaya, H., & Dheeraj, A. (2019). Experimental investigation on the abasement of operating temperature in solar photovoltaic panel using PCM and aluminium. *Solar Energy*, *188*, 327-338.

[28] Marudaipillai, S. K., Karuppudayar Ramaraj, B., Kottala, R. K., & Lakshmanan, M. (2023). Experimental study on thermal management and performance improvement of solar PV panel cooling using form stable phase change material. *Energy Sources, Part A: Recovery, Utilization, and Environmental Effects*, *45*(1), 160-177.

[29] Atkin, P., & Farid, M. M. (2015). Improving the efficiency of photovoltaic cells using PCM infused graphite and aluminium fins. *Solar Energy*, *114*, 217-228.

[30] Ma, T., Zhao, J., & Li, Z. (2018). Mathematical modelling and sensitivity analysis of solar photovoltaic panel integrated with phase change material. *Applied Energy*, *228*, 1147-1158.

[31] Durez, A., Ali, M., Waqas, A., Nazir, K., & Kumarasamy, S. (2023). Modelling and optimization of phase change materials (PCM)-based passive cooling of solar PV panels in multi climate conditions. *Frontiers in Energy Research*, *11*, 1121138.

[32] Al-Najjar, H. M. T., & Mahdi, J. M. (2022). Novel mathematical modeling, performance analysis, and design charts for the typical hybrid photovoltaic/phase-change material (PV/PCM) system. *Applied Energy*, *315*, 119027.

[33] Abdelrahman, H. E., Wahba, M. H., Refaey, H. A., Moawad, M., & Berbish, N. S. (2019). Performance enhancement of photovoltaic cells by changing configuration and using PCM (RT35HC) with nanoparticles Al2O3. *Solar Energy*, *177*, 665-671.

[34] Sharaf, M., Huzayyin, A. S., & Yousef, M. S. (2022). Performance enhancement of photovoltaic cells using phase change material (PCM) in winter. *Alexandria Engineering Journal*, *61*(6), 4229-4239.

[35] Praveen, B., & Suresh, S. (2018). Experimental study on heat transfer performance of neopentyl glycol/CuO composite solid-solid PCM in TES based heat sink. Engineering science and technology, an international journal, 21(5), 1086-1094.

[36] Singh, A. P., Khanna, S., Paneliya, S., Hinsu, H., Patel, Y., & Mehta, B. (2021). Preparation and characterization of solid-state neopentyl glycol/expanded graphite micro composite for thermal energy storage applications. *Materials Today: Proceedings*, *47*, 621-625.

[37] Wang, S., Sun, L., Li, B., & Dai, L. (2021). Atomistic insights into the anisotropic and low thermal conductivity in neopentyl glycol crystals: A molecular dynamics study. *The Journal of Physical Chemistry C*, *125*(29), 15853-15862.

[38] Wang, C., Li, Q., Wang, L., & Lan, X. (2016). Phase transition of neopentyl glycol in nanopores for thermal energy storage. *Thermochimica Acta*, *632*, 10-17.

[39] Krishnan, S. A., Suresh, S., Midhun, V. C., & Behera, S. R. (2023). Experimental investigation of nanoparticle enhanced polyol solid–solid phase change material aided heat sink with integrated heat pipe for electronic cooling application. *Thermal Science and Engineering Progress*, *46*, 102222.

[40] A. Fluent, "12.0 Theory Guide," *Ansys Inc*, 2009.

[41] Jiang, L., Cui, S., Sun, P., Wang, Y., & Yang, C. (2020, June). Comparison of monocrystalline and polycrystalline solar modules. In *2020 IEEE 5th Information Technology and Mechatronics Engineering Conference (ITOEC)* (pp. 341-344). IEEE.

[42] Lexron. (n.d.). Lexron 12-Watt Monocrystal Solar Panel. Retrieved from https://www.atakale.com/index.php?route=product/product&path=20_80&product_id=70

[43] Direnc.Net. (n.d.). 25 W Aluminum Resistance. Retrieved from https://www.direnc.net/33r-25w-aluminyum-direnc

[44] The Eppley Laboratory Inc., ”Black & White Pyranometer Model 8-48 Specifications”, Model 8-48 Datasheet, (n.d.).

[45] Keysight, “34970A Data Acquisition/Switch Unit Family Technical Overview”, Keysight 34972A Datasheet, Sep. 2020.

[46] Alnor, “”CompuFlow Thermo-anemometer Model 8570/8571”, Owner’s Manual, (n.d.).

[47] European Comission. (n.d.). Photovoltaic Geographycal Information System. Retrieved from https://re.jrc.ec.europa.eu/pvg_tools/en/#api_5.1

[48] Comark Probes,”Choosing Your Comark Probes”, Retrieved from https://www.farnell.com/datasheets/94331.pdf, (n.d.)

[49] Keysight, “N8700 Series System DC Power Supplies”, Keysight 8761A Datasheet, (n.d.).

[50] Optris, “Thermal Cameras”, PI400i Datasheet, (n.d.).

[51] Aluminum Thermopysical Properties. (n.d.). Engineering Tool Box. Retrieved from https://www.engineeringtoolbox.com/aluminum-specific-heat-density-thermal-conductivity-temperature-d_2220.html

[52] Bergman, T. L. (2011). *Fundamentals of heat and mass transfer*. John Wiley & Sons.

[53] Khanna, S.; Reddy, K.S.; Mallick, T.K. Performance analysis of tilted photovoltaic system integrated with phase change material under varying operating conditions. Energy 2017, 133, 887–899.

[54] Santbergen, R., & van Zolingen, R. C. (2008). The absorption factor of crystalline silicon PV cells: A numerical and experimental study. *Solar energy materials and solar cells*, *92*(4), 432-444.

[55] Skoplaki, E., & Palyvos, J. A. (2009). On the temperature dependence of photovoltaic module electrical performance: A review of efficiency/power correlations. *Solar energy*, *83*(5), 614-624.

[56] Sharples, S., & Charlesworth, P. S. (1998). Full-scale measurements of wind-induced convective heat transfer from a roof-mounted flat plate solar collector. *Solar Energy*, *62*(2), 69-77.

[57] Gardon, R. (1956). The emissivity of transparent materials. *Journal of the American Ceramic Society*, *39*(8), 278-285.

[58] Voller, V. R., & Swaminathan, C. R. (1991). ERAL Source-based method for solidification phase change. Numerical Heat Transfer, Part B Fundamentals, 19(2), 175-189.

[59] Voller, V. R., Cross, M., & Markatos, N. C. (1987). An enthalpy method for convection/diffusion phase change. International journal for numerical methods in engineering, 24(1), 271-284.

[60] Al-Waeli, A. H., Chaichan, M. T., Sopian, K., Kazem, H. A., Mahood, H. B., & Khadom, A. A. (2019). Modeling and experimental validation of a PVT system using nanofluid coolant and nano-PCM. *Solar Energy*, *177*, 178-191.

[61] Choudhari, V. G., Dhoble, A. S., & Panchal, S. (2020). Numerical analysis of different fin structures in phase change material module for battery thermal management system and its optimization. International Journal of Heat and Mass Transfer, 163, 120434.